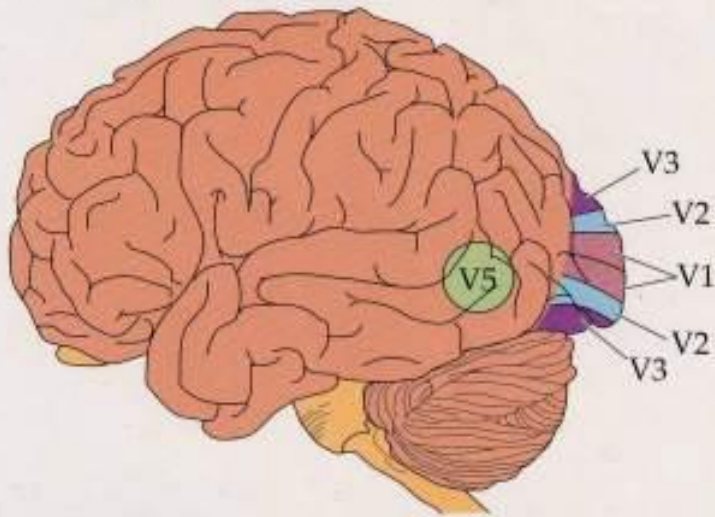
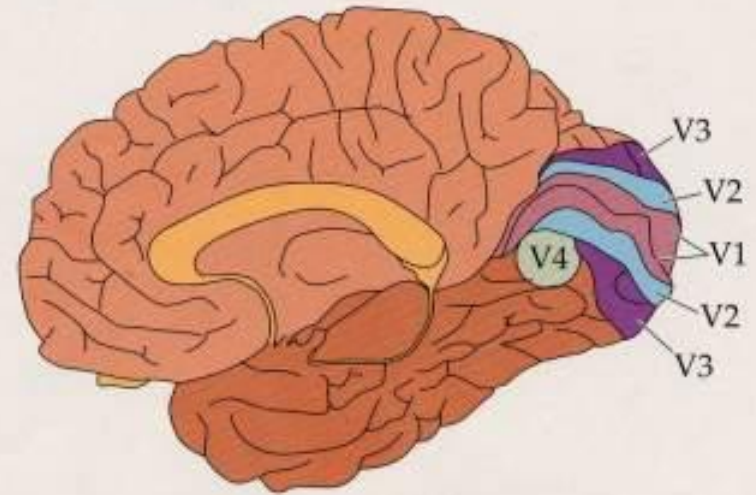


Some Human Cortical Visual Regions: V1, V2, V3, V4, V5 (MT)

(e) Human brain, lateral view



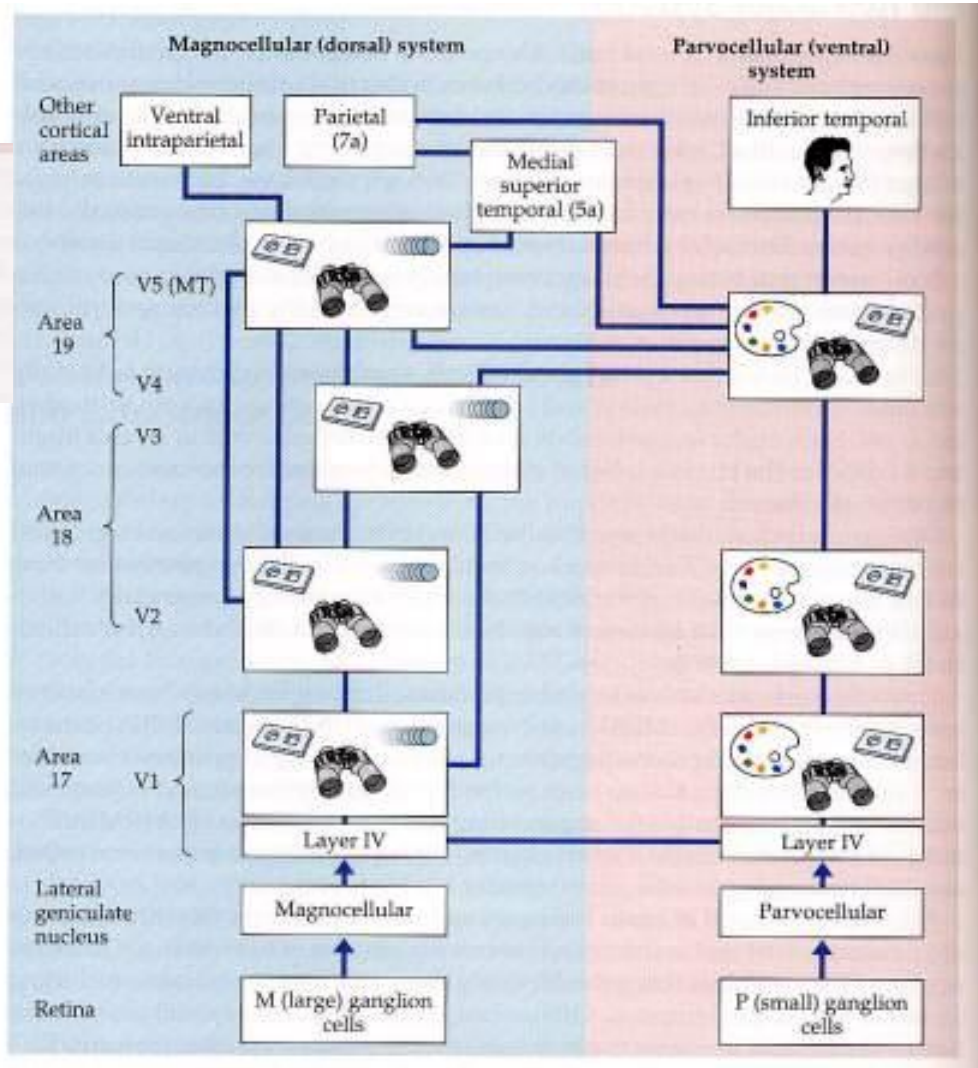
(d) Human brain, medial view



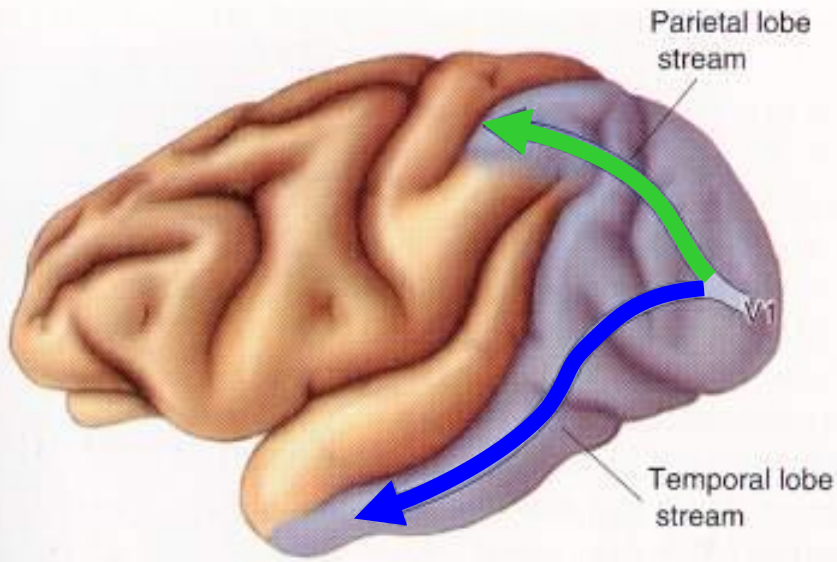
Retinal and Thalamic Precursors of the Dorsal and Ventral Visual Pathways



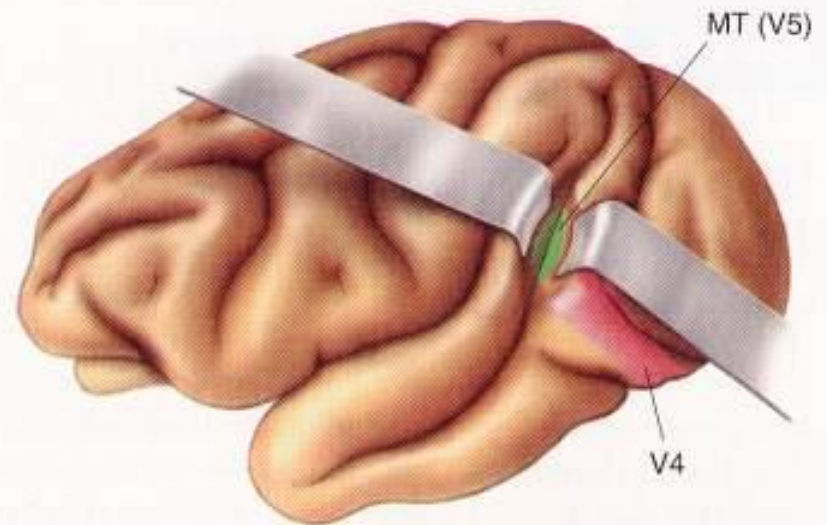
Magnocellular (dorsal) and parvocellular (ventral) pathways from the retina to the higher levels of the visual cortex are separate at the lower levels of the visual system. At higher levels they show increasing overlap.



Dorsal (“Where”) and Ventral (“What”) Visual Streams in Monkey

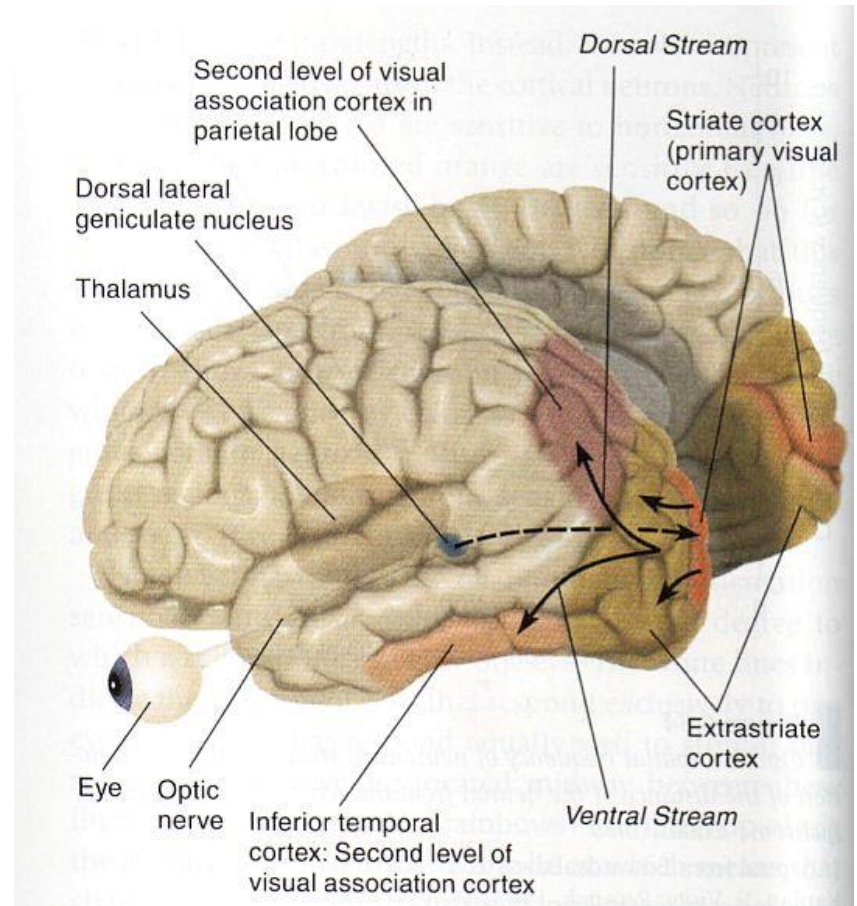
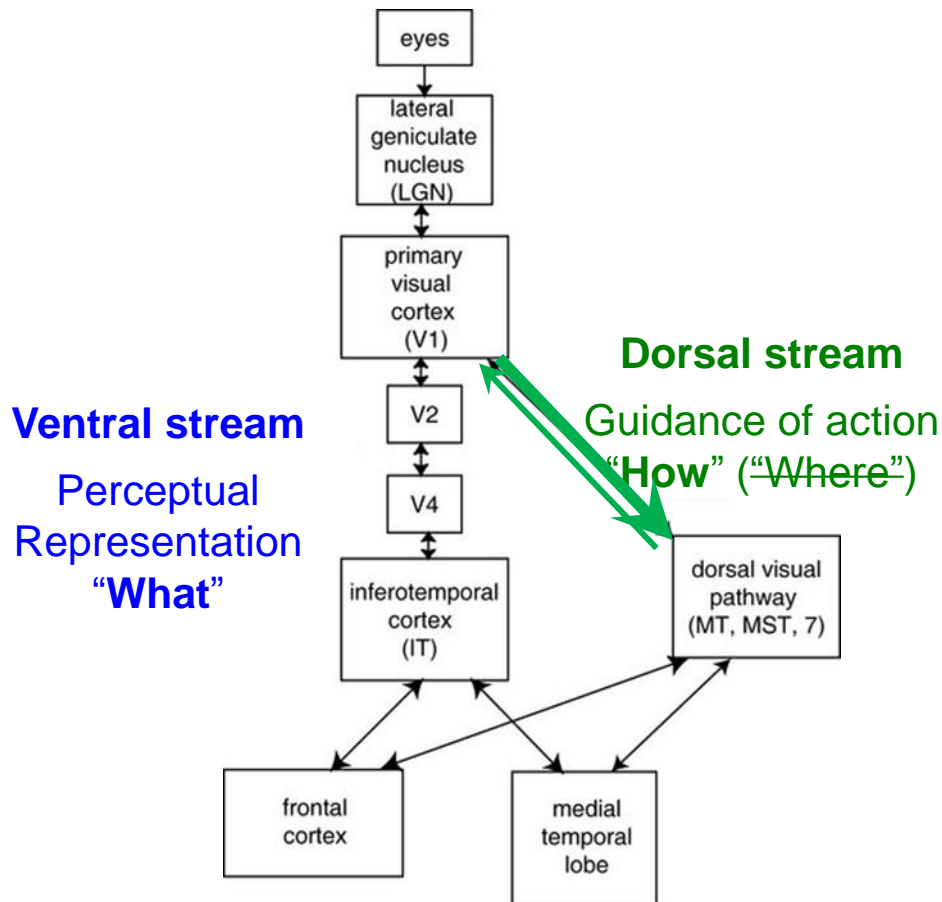


Parietal (Dorsal) and Temporal (Ventral) Processing Streams



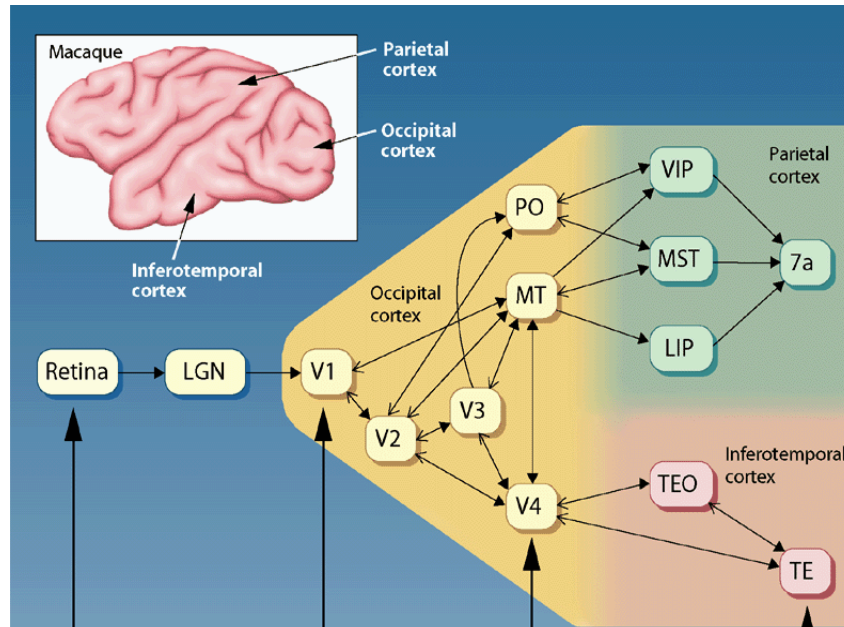
Areas MT and V4 in the Macaque Brain

Dorsal and Ventral Visual Streams



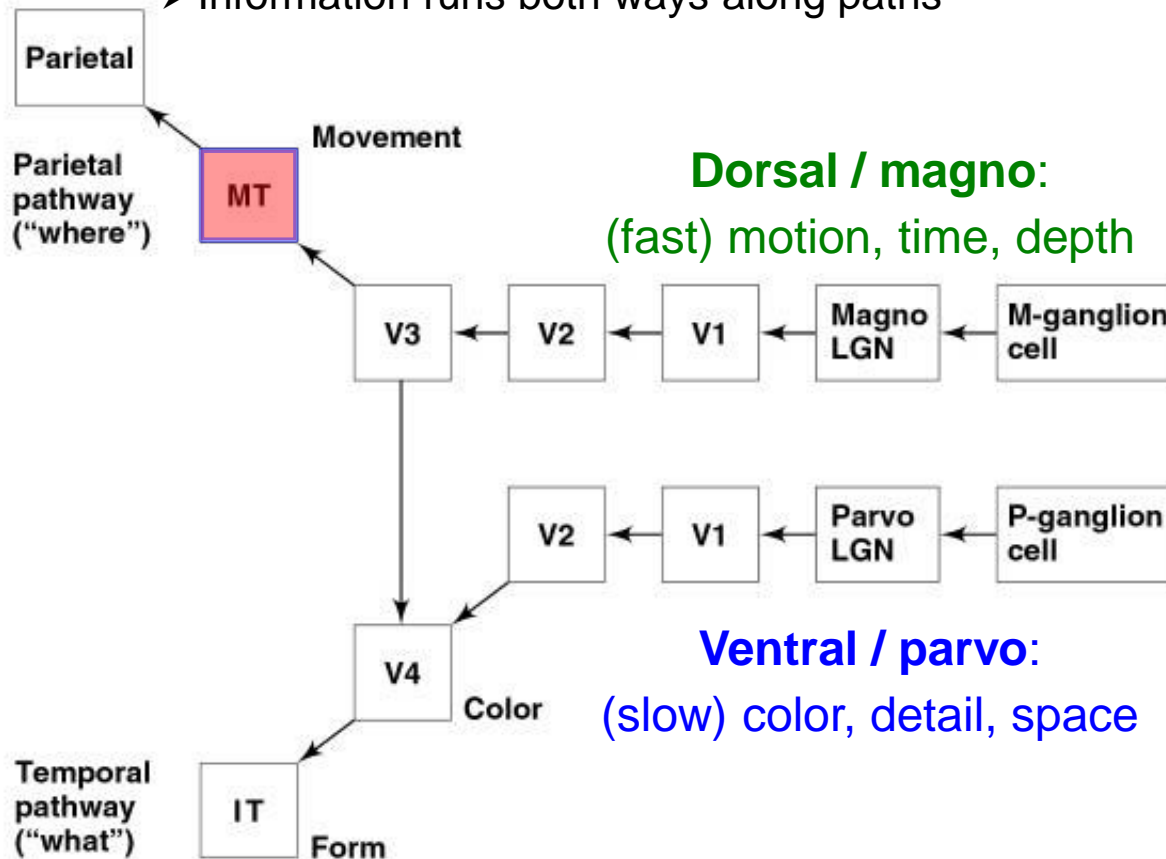
The Role of *Extrastriate* Areas

- Different visual cortex regions contain cells with different tuning properties that represent different features in the visual field
- V5/MT is selectively responsive to motion
- V4 is selectively responsive to color



Visual Pathways

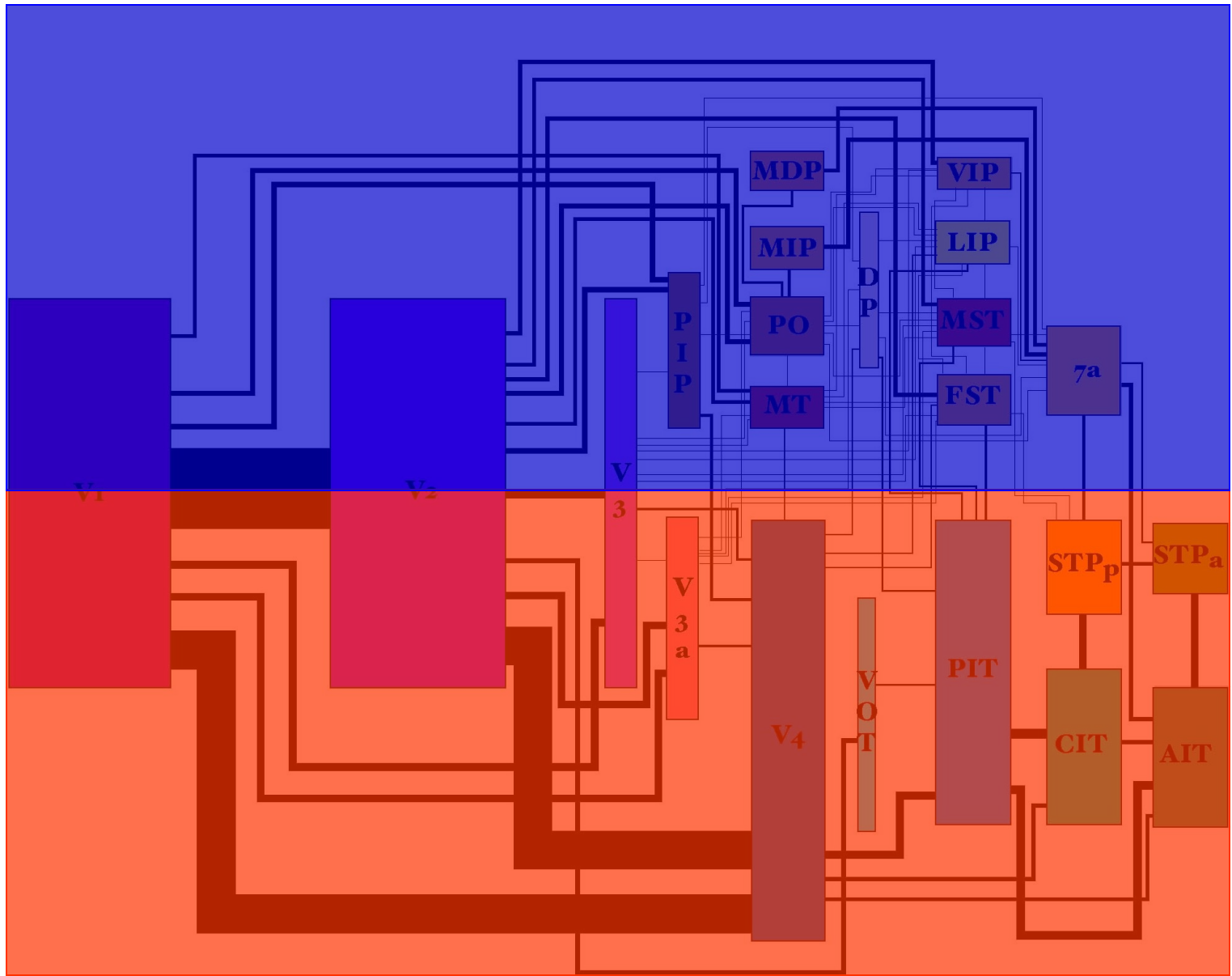
- The two pathways originate in the retina, have special zones in the LGN, and are treated differently in the extra-striate areas
- The two pathways are weakly modular at best (they do not operate independently but have interconnections – *cross talk* – at every level)
 - Difference of function vs. modularity of function
 - Information runs both ways along paths



Magno- and Parvo-ganglion cells in the retina are physically and functionally distinct neurons.

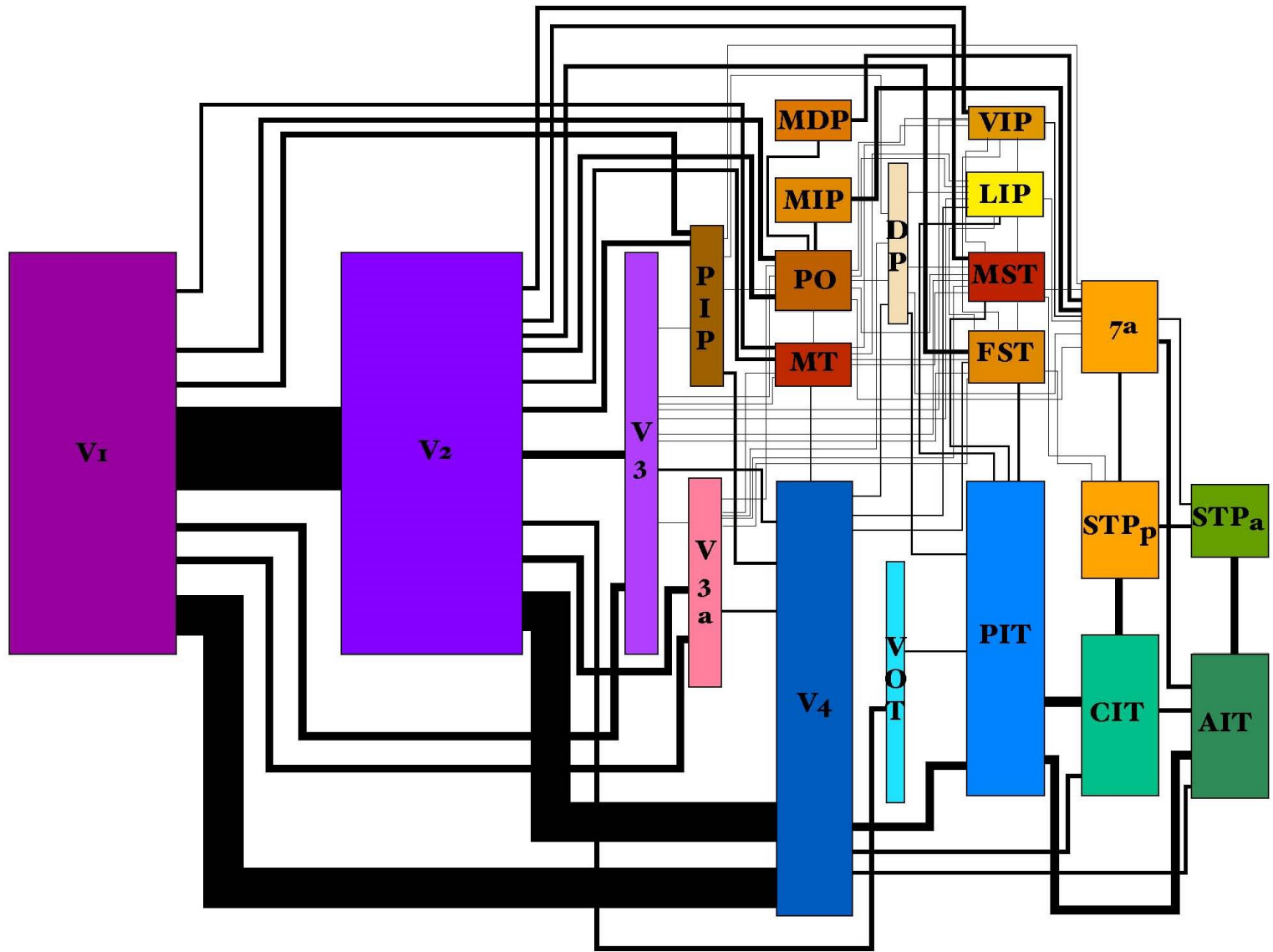
DORSAL

VENTRAL

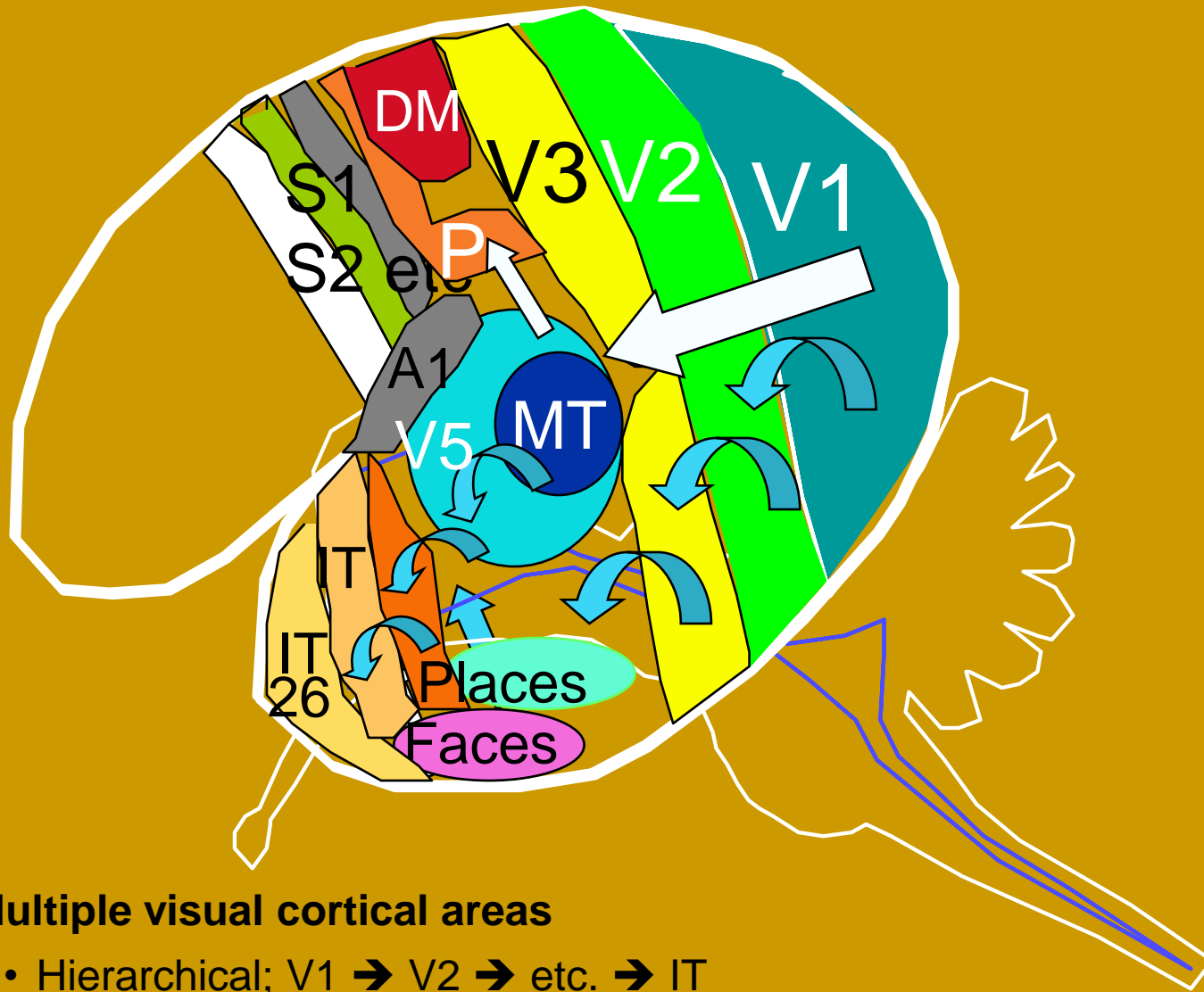


The size of each area is proportional to its cortical surface area. The thickness of the connection lines represents **feedforward connections only**, based on the rule that an area has a number of output connections proportional to its area, and that these are divided among its target areas in proportion to their relative areas. In other words, *all connections are presumed equal in strength*. Some of the weaker connections have been thickened a little to make them more visible. Areas are arranged left to right according to the hierarchical rules of Felleman and Van Essen (1991, *Cerebral Cortex*). *By Tony Movshon based on a suggestion of Peter Lennie (Perception Lecture, ECVF 1998; see Wallisch & Movshon, Neuron 2008).*

DORSAL
VENTRAL



The size of each area is proportional to its cortical surface area. The thickness of the connection lines represents **feedforward connections only**, based on the rule that an area has a number of output connections proportional to its area, and that these are divided among its target areas in proportion to their relative areas. In other words, *all connections are presumed equal in strength*. Some of the weaker connections have been thickened a little to make them more visible. Areas are arranged left to right according to the hierarchical rules of Felleman and Van Essen (1991, *Cerebral Cortex*). *By Tony Movshon based on a suggestion of Peter Lennie (Perception Lecture, ECVF 1998; see Wallisch & Movshon, Neuron 2008).*



Dorsal Stream

- V1, MT, DM, P
- Precision place
- “Where/ How?”
- M system
- Unconscious
- Veridical
- No illusions

Ventral Stream

- V1, V2, V3,IT
- Object identification
- “What?”
- P system
- Conscious
- Abstract
- Illusions

Multiple visual cortical areas

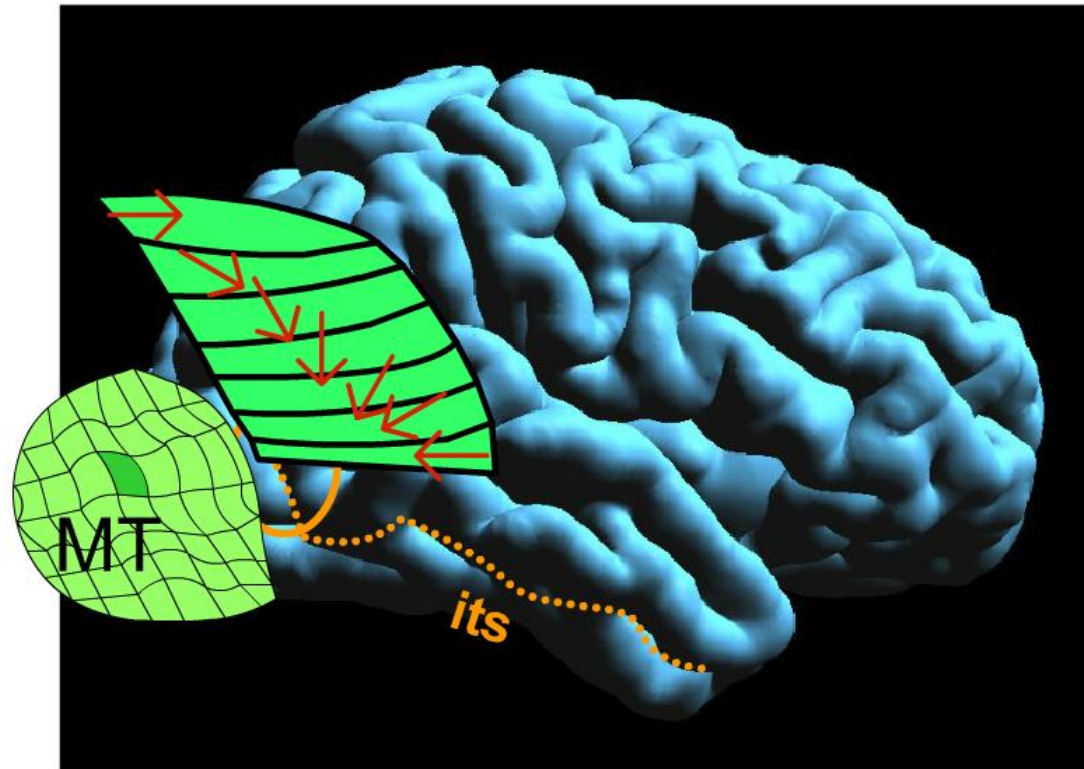
- Hierarchical; V1 → V2 → etc. → IT
- Multiply interconnected
- “Apex” of hierarchy is hippocampal cortex
- Each has complete representation of visual field
- Functional specialisation (colour, motion, depth, etc.)

MT, like V1, is organized into columns.

One particular column receives input from one patch of retina

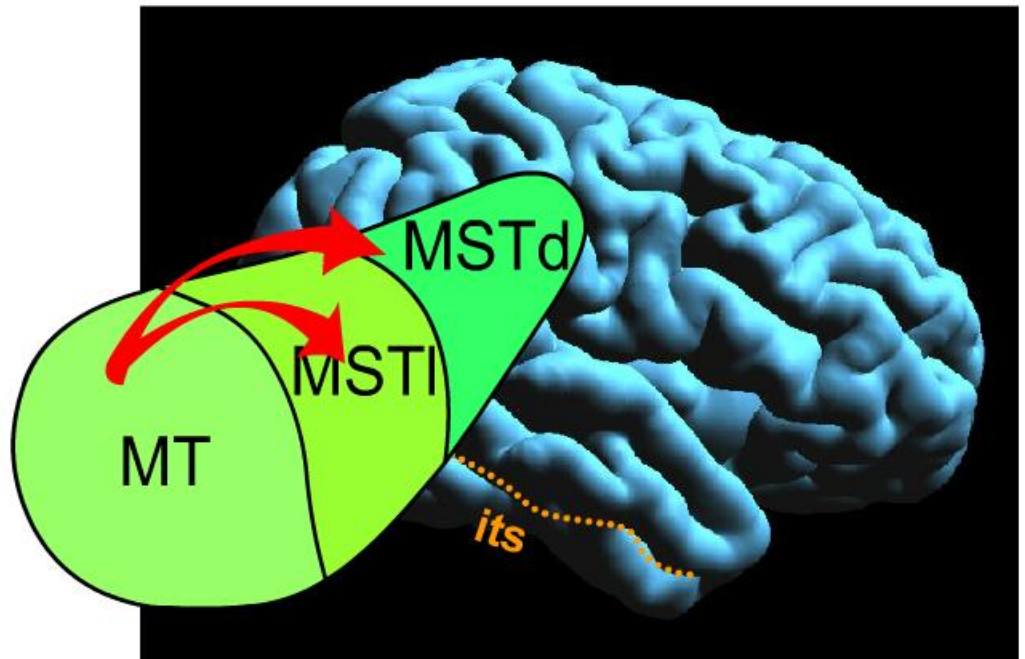
The column is further subdivided into areas tuned for a particular direction of motion.

Neighboring regions prefer slightly different directions of motion



MT then sends motion information to MST

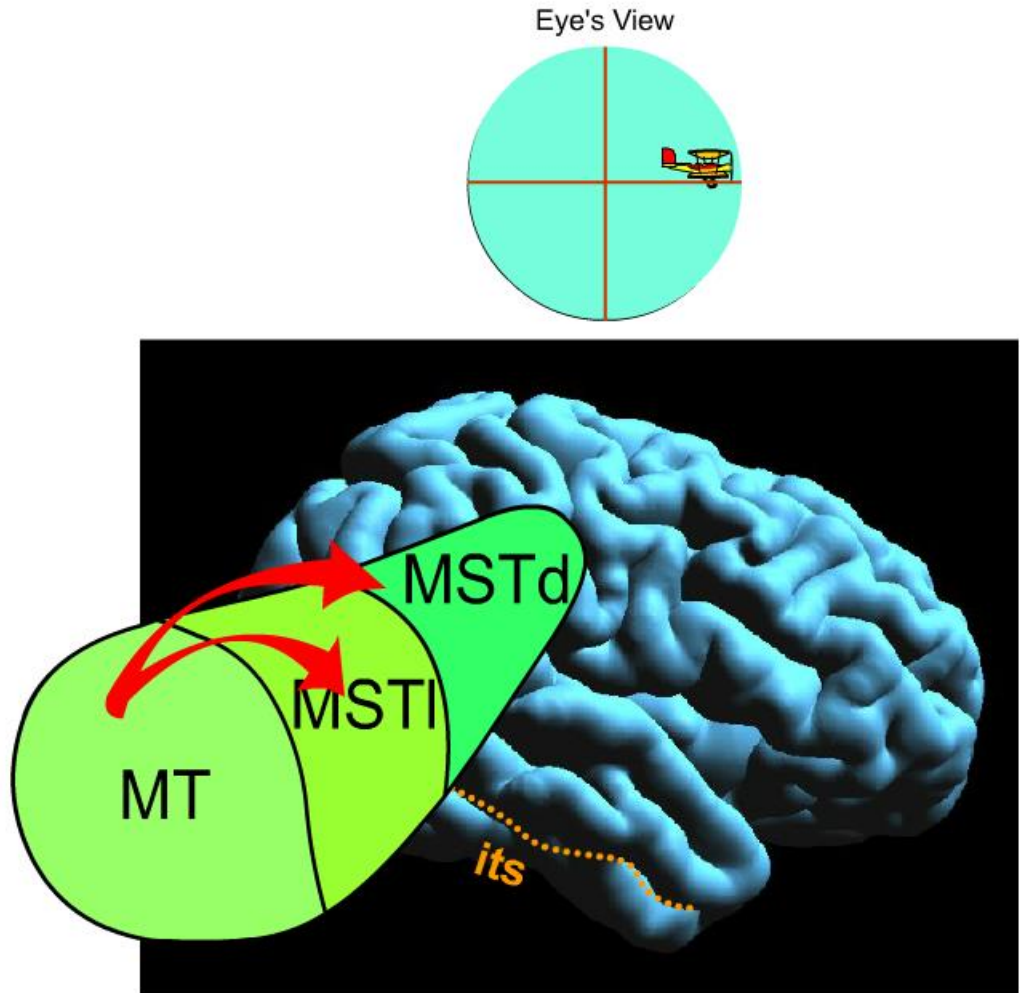
MST is subdivided into a dorsal, MSTd, and lateral part, MSTl. These analyse two basic types of visual motion.



MT then sends motion information to MST

MSTl senses when objects move.

Often these objects are small activating small parts of the retina.

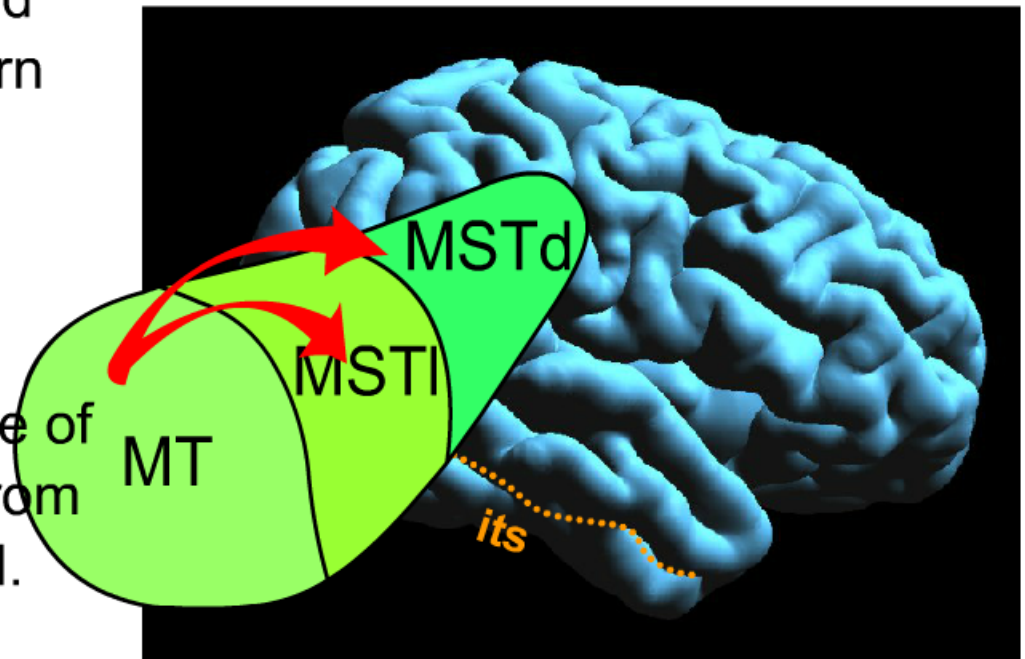
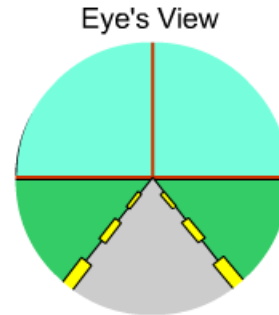


MT then sends motion information to MST

MSTd senses the visual motion produced when you move.

In this case, movement of the background produces an optic flow pattern on the entire retina.

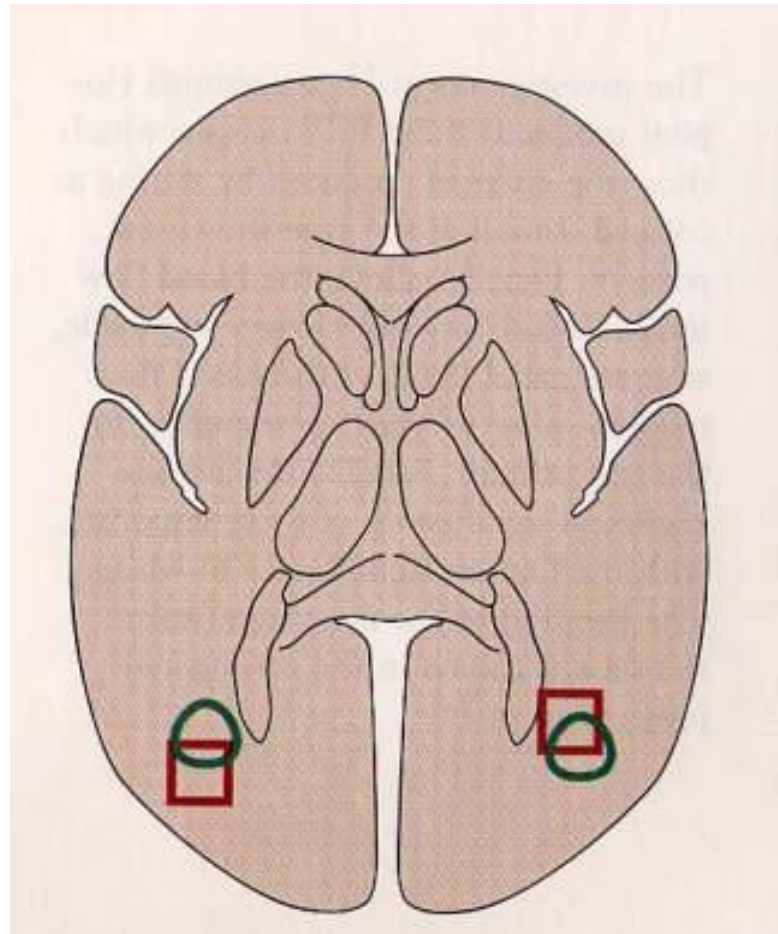
MSTd neurons have receptive fields that are much larger than those of MT, often integrating motion from almost the entire visual field.



They are organized in columns with each column tuned to different optic flow types (translation, rotation, expansion, contraction)

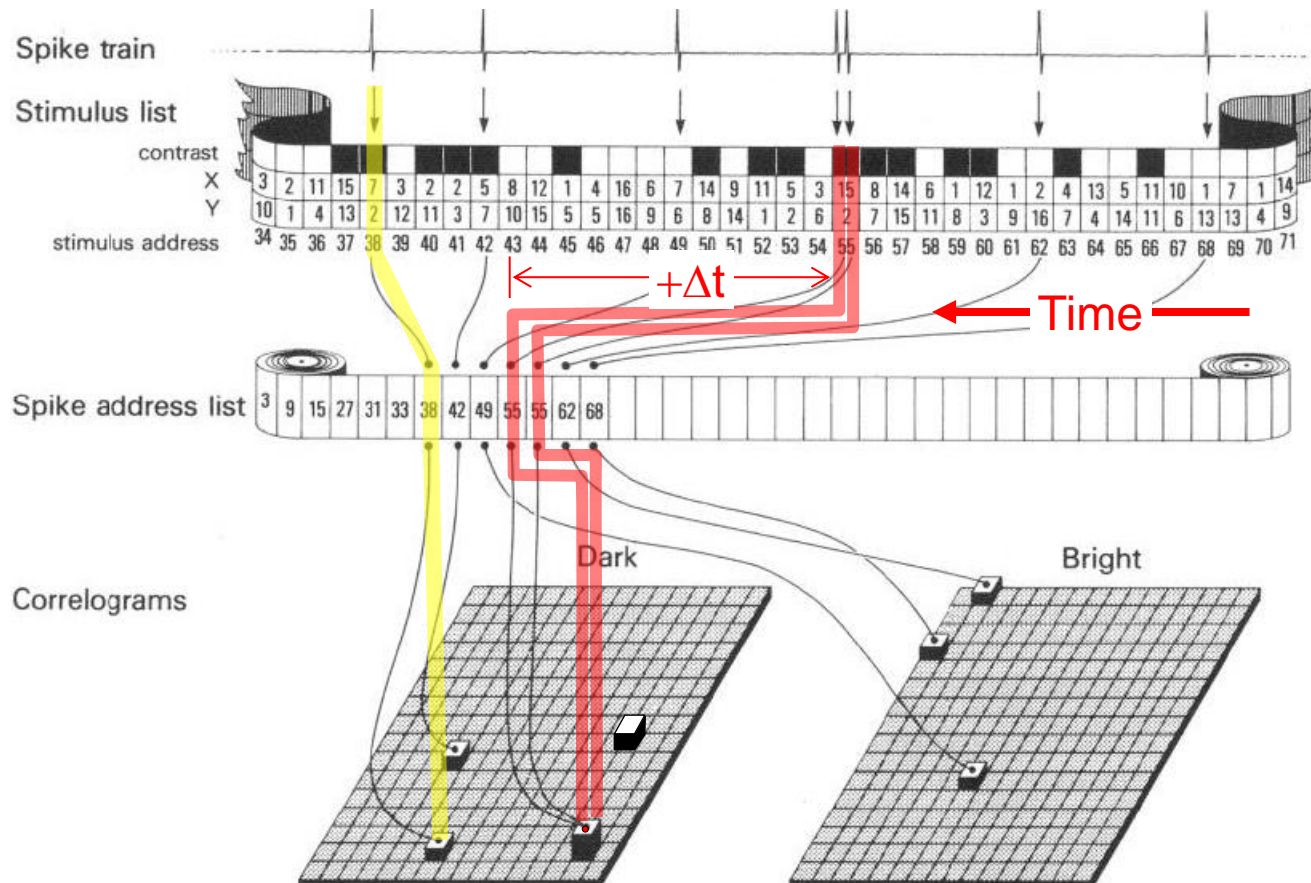
PET Identification in Humans of Cortical Region MT for Motion Perception

A single slice shows the location of MT found by Frackowiak and Zeki in London (**red squares**) and Miezen, Petersen, and Fox in St. Louis (**green circles**). The areas of activation in the extrastriate cortex almost superimpose.



Reverse Correlation - Physiology

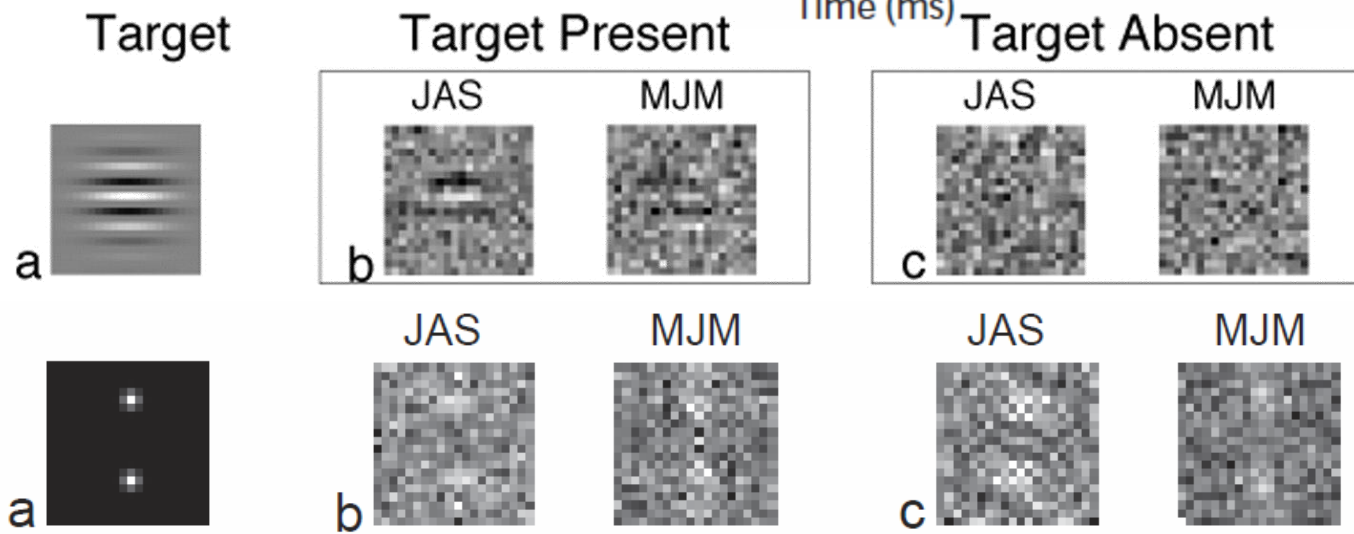
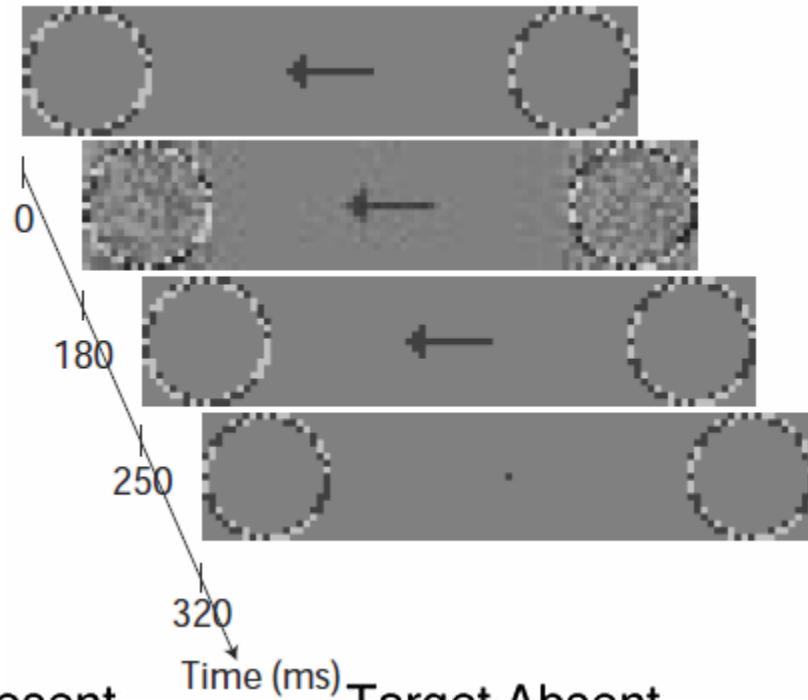
In the white-noise approach to RF mapping, a rapid, pseudo-random stimulus sequence that consists of patterns of spots or bars is presented, and the neuronal spike train is correlated to the stimulus sequence (that is, cross- or reverse-correlation). The aim of this correlation procedure is to characterize the transformation that occurs between the visual stimulus and the response of a neuron (that is, the neuron's 'transfer function'). Because stimuli are presented in rapid succession, without pausing to collect the response to each pattern, this technique is fast.



Reverse Correlation - Psychophysics

Solomon (2002) *J. Vision.*, 2, 105-120.

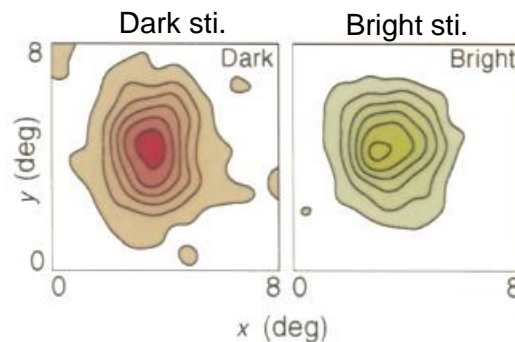
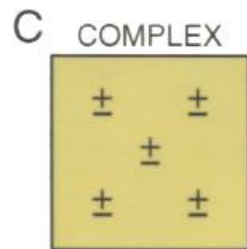
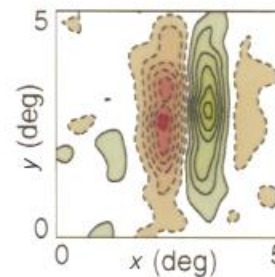
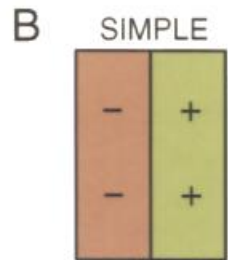
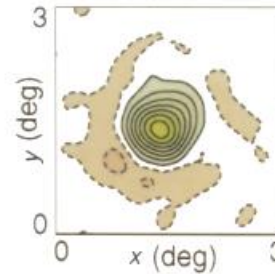
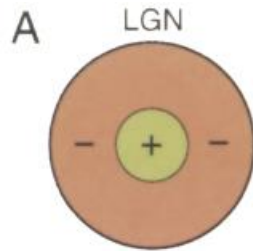
		STIMULUS	
		Noise	Signal
RÉPONSE	Yes	FA	Hit
	No	CR	Miss



Receptive field (RF) *spatial* structure of the major classes of neurons in the geniculostriate pathway of the cat

Schematic RF

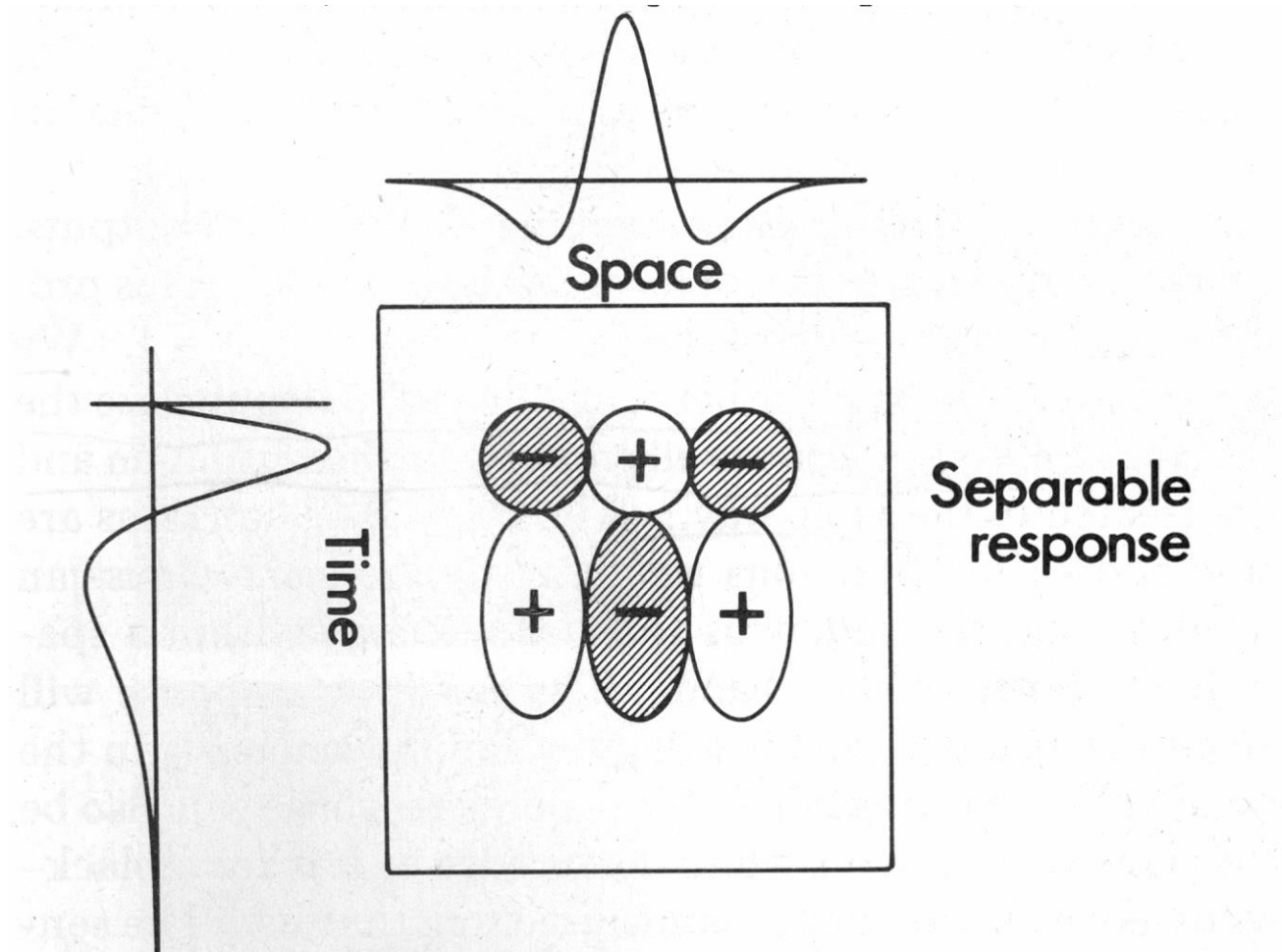
Measured RF
(Rev. Correl.)



Area 17

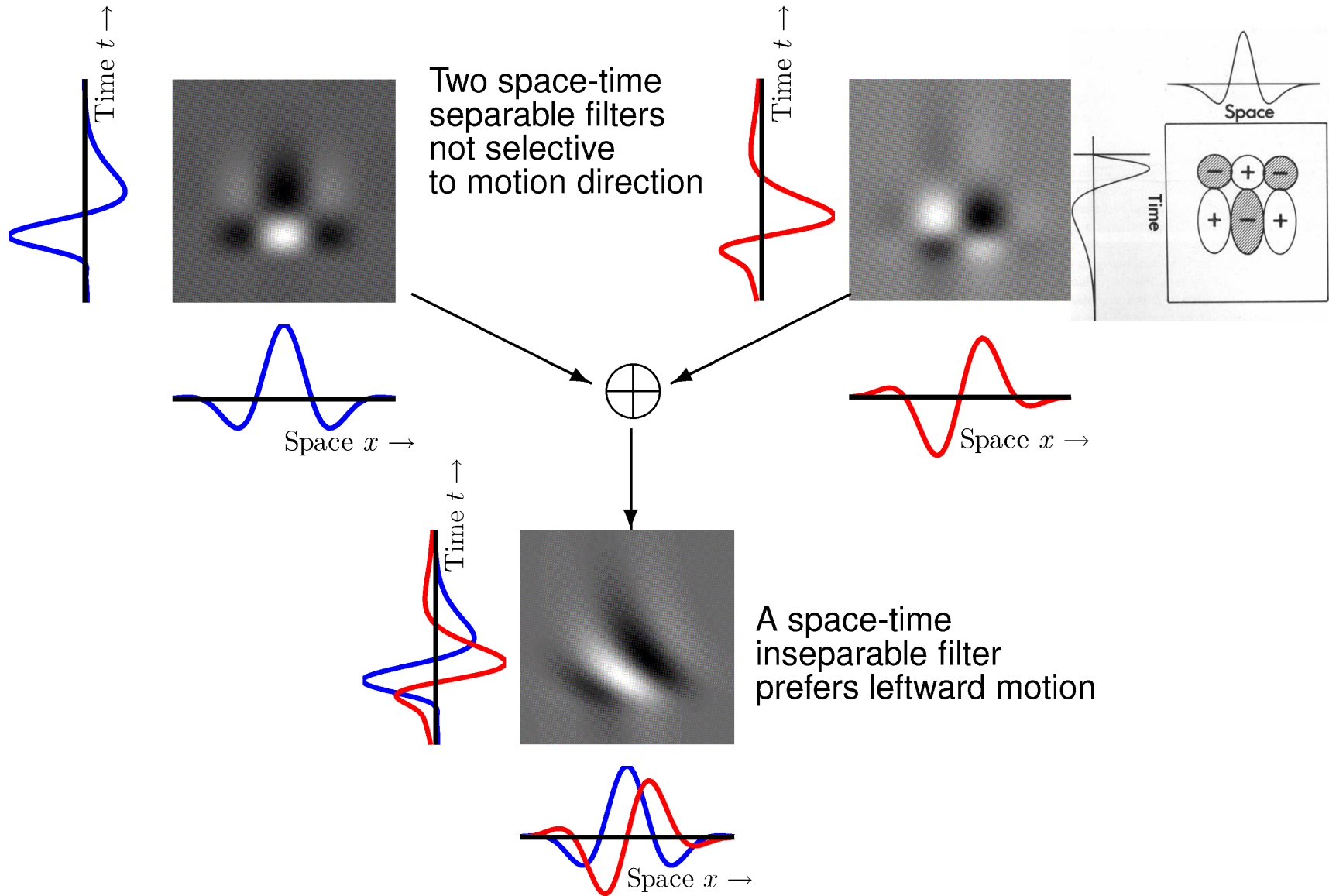
Motion “Energy”

Non-oriented Spatio-Temporal RF

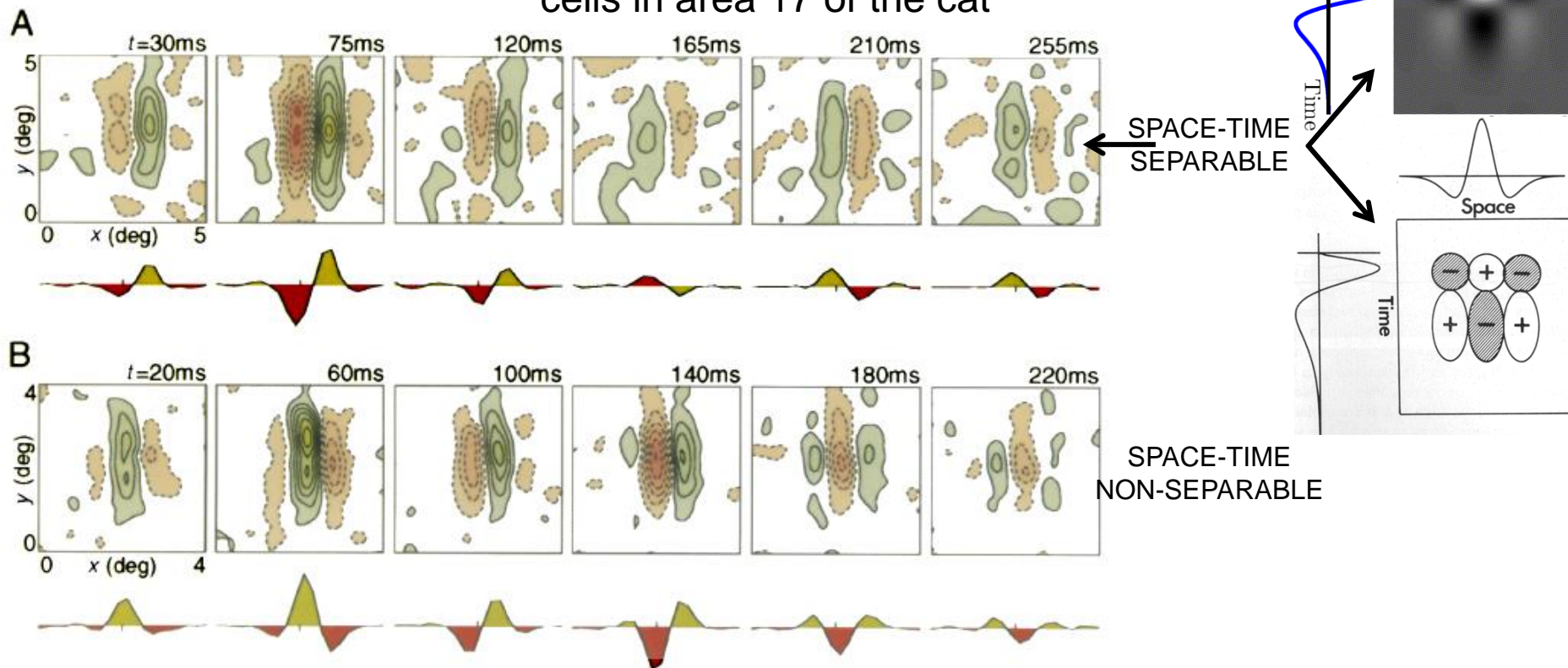


Adelson, E. H. & Bergen, J. R. (1985). Spatiotemporal energy models for the perception of motion. *J. Opt. Soc. Am. A* 2, 284-299.

Quadrature model of motion direction selectivity

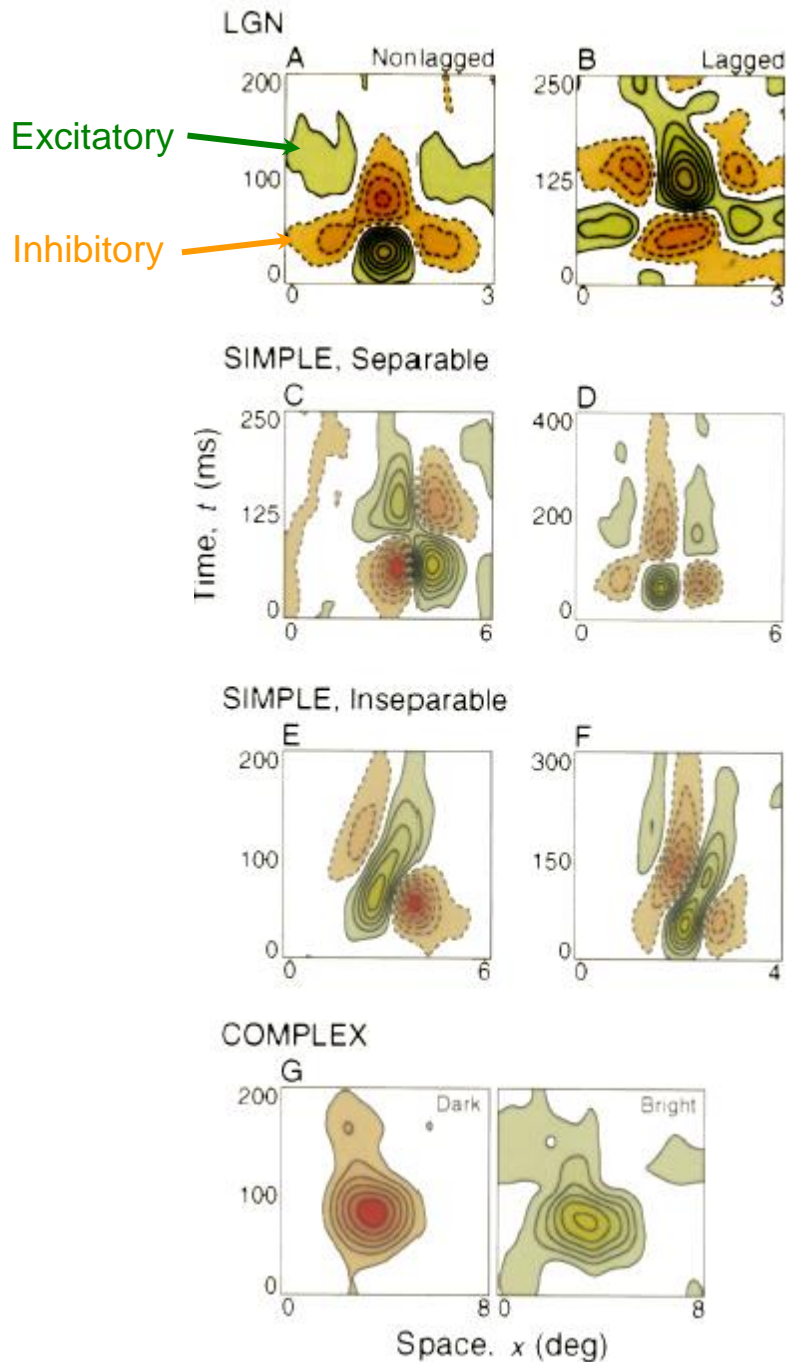


Receptive field (RF) *spatial* structure over *time* of simple cells in area 17 of the cat



Dynamics of receptive field (RF) structure of simple cells from striate cortex of the cat. By varying the correlation delay, t , in the RF mapping algorithm, 'snapshots' of the RF can be obtained at different times relative to stimulus onset. These data were obtained using a reverse correlation technique. For each cell, two-dimensional (2D) spatial (x-y) RF profiles are shown, as isoamplitude contour maps (conventions as in Fig. 1), for six values of t . Below each contour plot is a 1D RF profile that is obtained by integrating the 2D profile along the y axis, which is parallel to the cell's preferred orientation. Positive deflections (shaded green) in these 1D profiles indicate bright-excitatory subregions; negative deflections (shaded red) correspond to dark-excitatory subregions. **(A)** The RF of this simple cell is approximately space-time separable. From $t = 30$ ms to $t = 120$ ms, the RF profile has two dominant subregions, which are arranged with the dark-excitatory subregion on the left. These subregions are strongest at $t = 75$ ms. Between $t = 120$ ms and $t = 165$ ms, the RF reverses polarity, so that the bright-excitatory subregion is now on the left. This arrangement then persists over the remainder of the cell's response duration. Note that, at all values of t , the 1D RF profile is approximately odd symmetric (sine phase). **(B)** A fundamentally different type of spatiotemporal behavior is illustrated here. For this cell, the RF is space-time inseparable - the spatial organization of the RF changes over time. At $t = 20$ ms, the 1D profile is approximately even symmetric (cosine phase) whereas, at $t = 100$ ms, the RF profile is odd symmetric. Later, at $t = 180$ ms, the RF becomes even symmetric again but the profile is inverted relative to that at $t = 20$ ms.

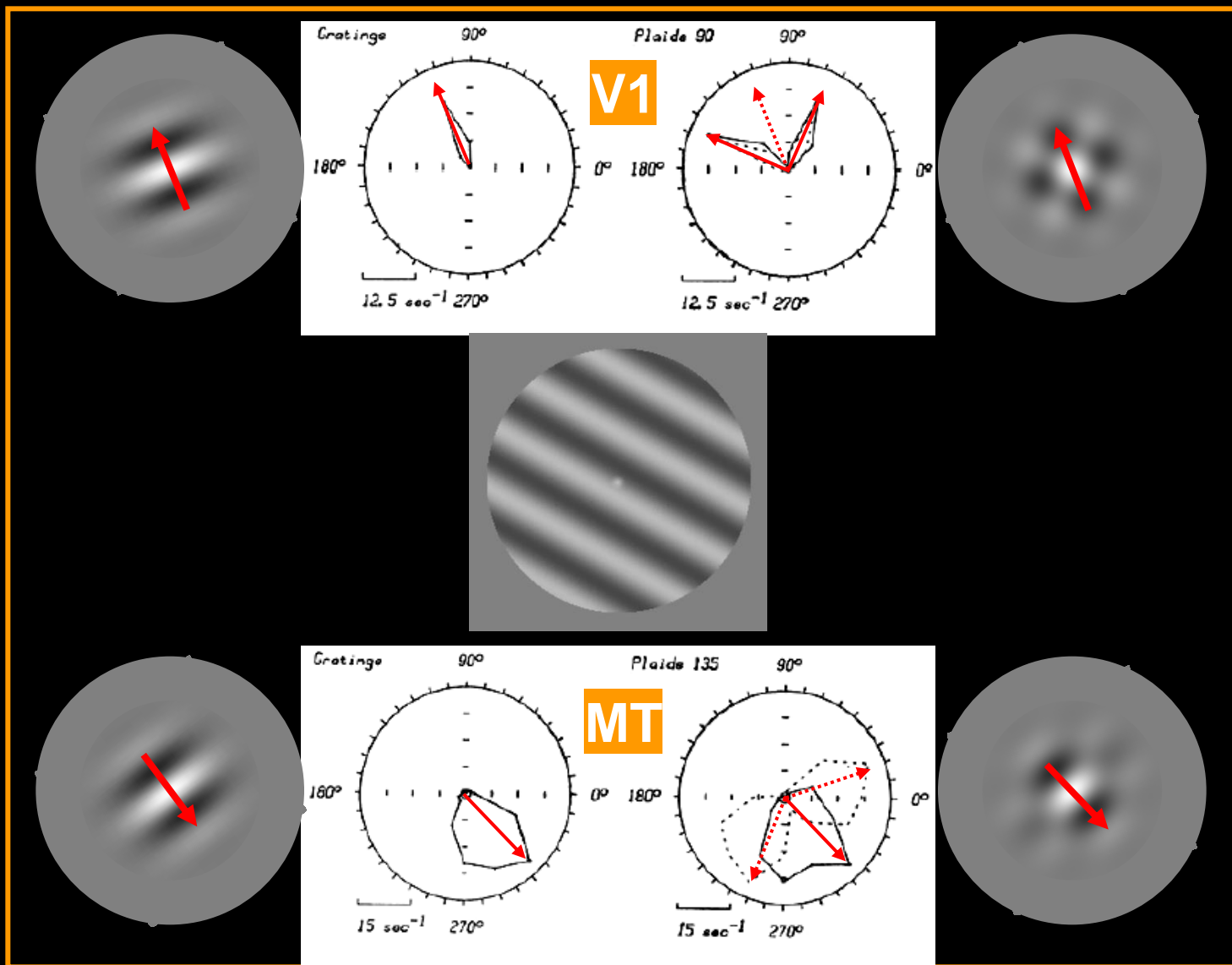
Spatiotemporal receptive field (RF) profiles (x-t plots) for neurons in the lateral geniculate nucleus (LGN) and striate cortex of the cat.

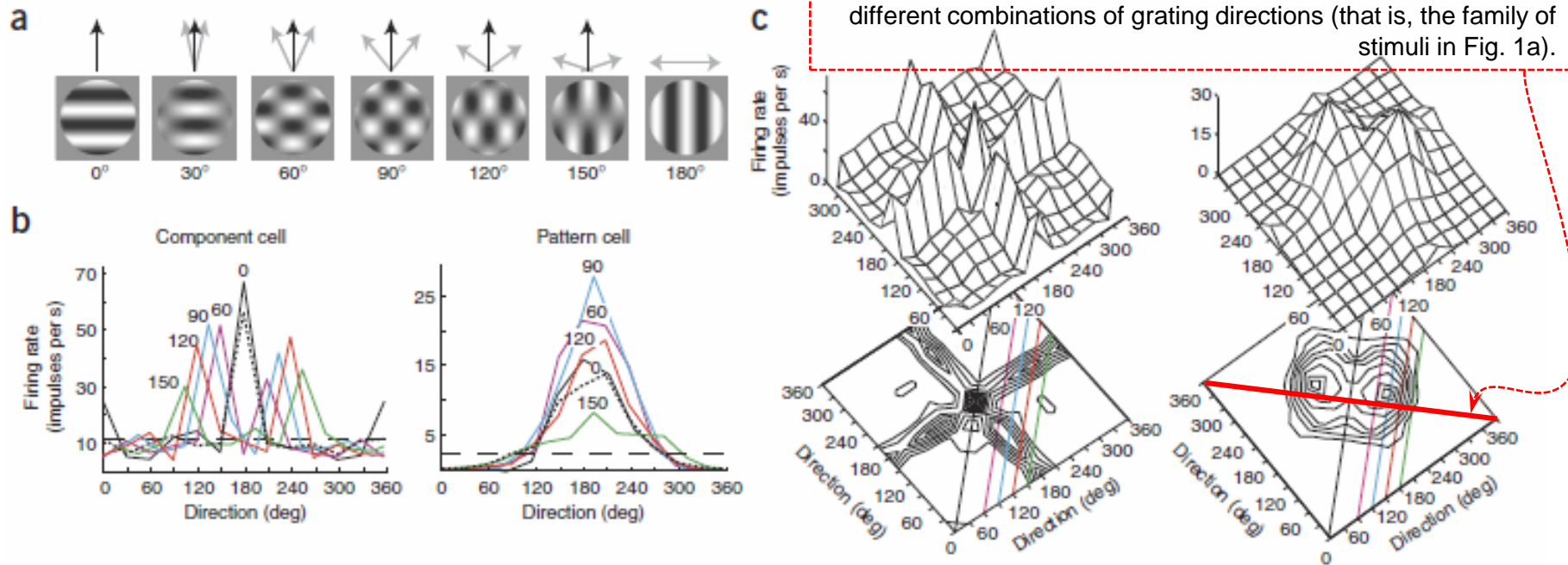


In each panel, the horizontal axis represents space (x), and the vertical axis represents time (t). For panels A-F, solid contours (with green shading) delimit bright-excitatory regions, whereas broken contours (with red shading) indicate dark-excitatory regions. To construct these x-t plots, 1D RF profiles are obtained, at finely spaced time intervals (5-10ms), over a range of values of t. These 1D profiles are then 'stacked up' to form a surface, which is smoothed and plotted as a contour map. (A) An x-t profile is shown here for a typical ON-center, non-lagged X-cell from the LGN. For $t < 50$ ms, the RF has a bright-excitatory center and a dark-excitatory surround. However, for $t > 50$ ms, the RF center becomes dark-excitatory, and the surround becomes bright-excitatory. (B) An x-t plot of an ON-center, lagged X-cell. Note that the second temporal phase of the profile is strongest. (C) An x-t profile for a simple cell with a space-time separable RF. For $t < 100$ ms, the RF has a dark-excitatory subregion to the left of a bright-excitatory subregion. For $t > 100$ ms, each subregion reverses polarity, so that the bright-excitatory region is now on the left. (D) Data for another simple cell with an approximately separable x-t profile. (E) Data are shown for a simple cell with a clearly inseparable x-t profile. Note how the spatial arrangement of bright- and dark-excitatory subregions (that is, the spatial phase of the RF) changes gradually with time. (F) An inseparable x-t profile is shown here for the same simple cell for which 2D spatial profiles are shown in Fig. 2B. Note that the subregions are tilted to the right in the space-time domain. (G) x-t profiles are shown for the same complex cell as in Fig. 1C. Responses to bright and dark stimuli are shown separately because these regions overlap extensively.

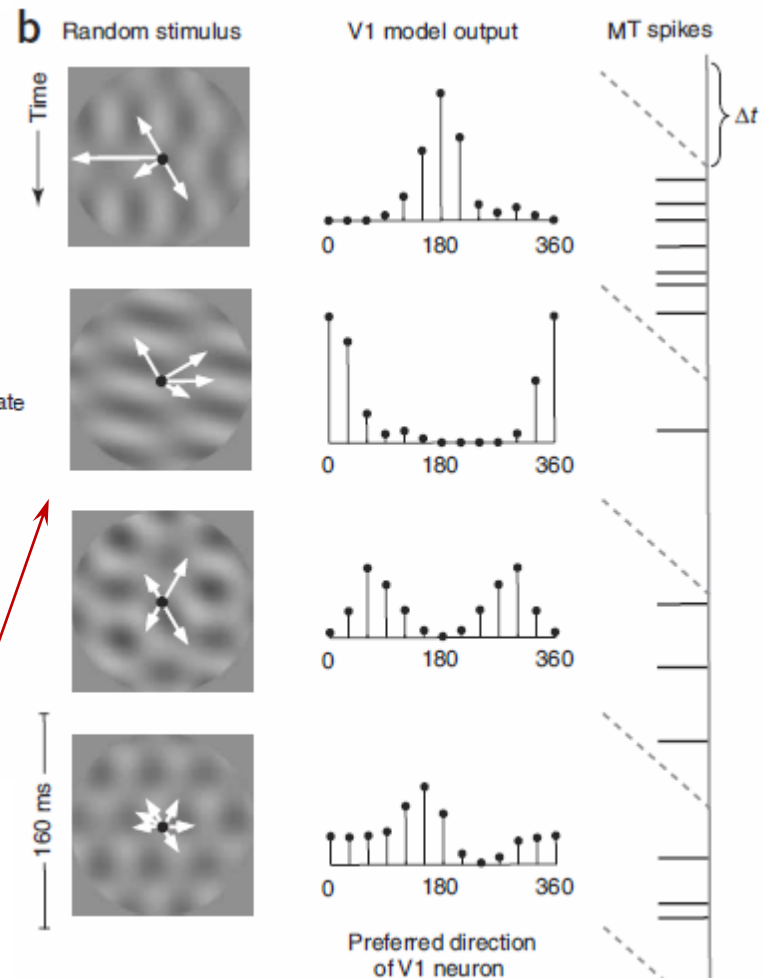
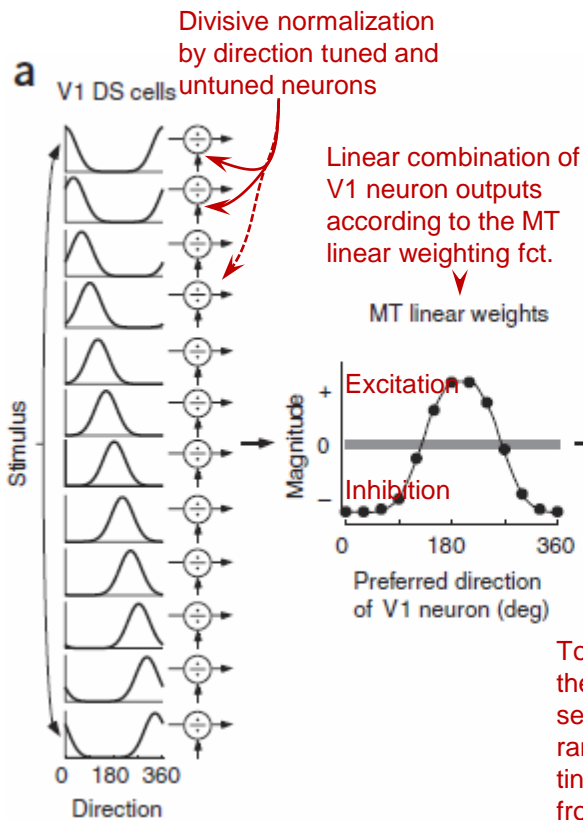
Coding locality in space-time and frequency

V1 & MT responses (Movshon et al., 1983)





Component and pattern MT cell responses to plaid stimuli. (a) Example plaid stimuli. All plaids were constructed by superimposing two sinusoidal gratings of equal contrast (contrast $\frac{1}{4}$ $\frac{1}{6}$), moving at the same spatial and temporal frequency. Gray arrows show the motion directions of the two gratings; black arrows show the motion direction of the plaid. The angular separation between the two gratings (the plaid angle) is given below each stimulus. When the plaid angle is zero, the gratings form a single grating with twice the contrast. (b) Direction tuning curves for example component (left) and pattern (right) cells, collected for plaids with different plaid angles. Each colored tuning curve represents the response to a particular plaid. For the component cell on the left, the functions have two peaks, displaced from one another by the angle of the plaid; for the pattern cell on the right, all have similar shapes and preferred directions. Also shown is the half-contrast grating tuning curve (black dotted line). (c) Surface and contour plots of response as a function of the direction of the two grating components. The colored lines in c indicate the loci of the particular plaids whose responses are shown in the same colors in b. Each direction interaction plot is symmetrical about the main diagonal (a plaid constructed from gratings 01 and 1201 gratings is equivalent to a plaid constructed from 1201 and 01 gratings). In the contour plots, contours begin at 20% of the maximum firing rate and subsequent contours indicate 10% increments.



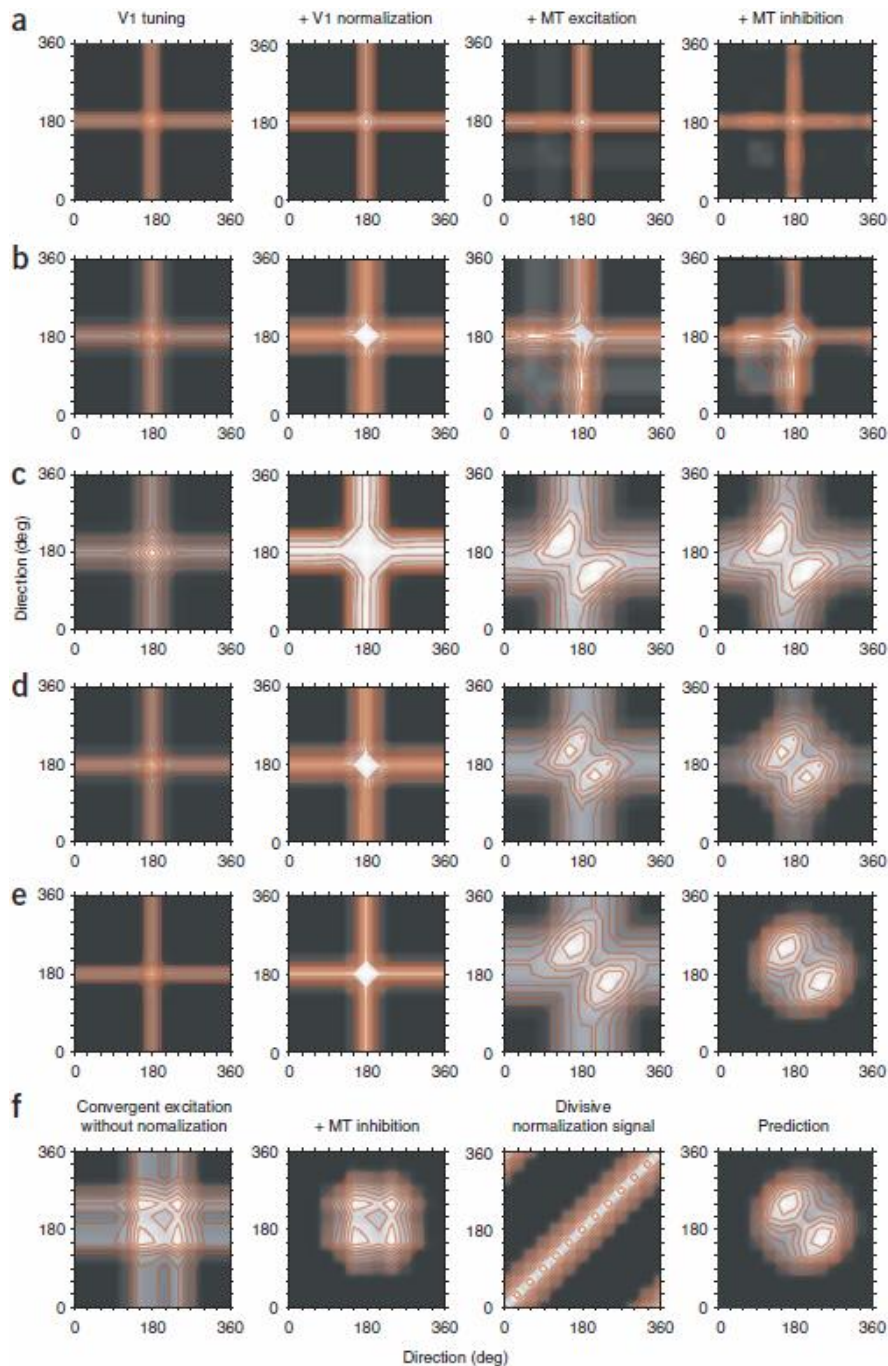
Model parameters

- V1 direction bandwidth
- Weights for the 2 normalization components
- Exponent of the nonlinear transform

To recover the components of the model, we presented a sequence of stimuli containing random combinations of 6 gratings, chosen with replacement from a pool of 12 gratings drifting in different directions. Arrows indicate the grating components randomly selected on a particular trial; longer arrows indicate the selection of more than one grating drifting in the same direction. After 160 ms, another set of 6 randomly selected gratings was immediately presented.

160ms by 160ms response of each of the 12 V1 cells in **a**.

Hypothetical spike train of an MT cell in response to the random grating stimulus. The spikes were shifted by the latency of the cell's response (Δt) and the number of spikes occurring in a 160-ms bin counted. The cascade model is then fit to these spike count data.

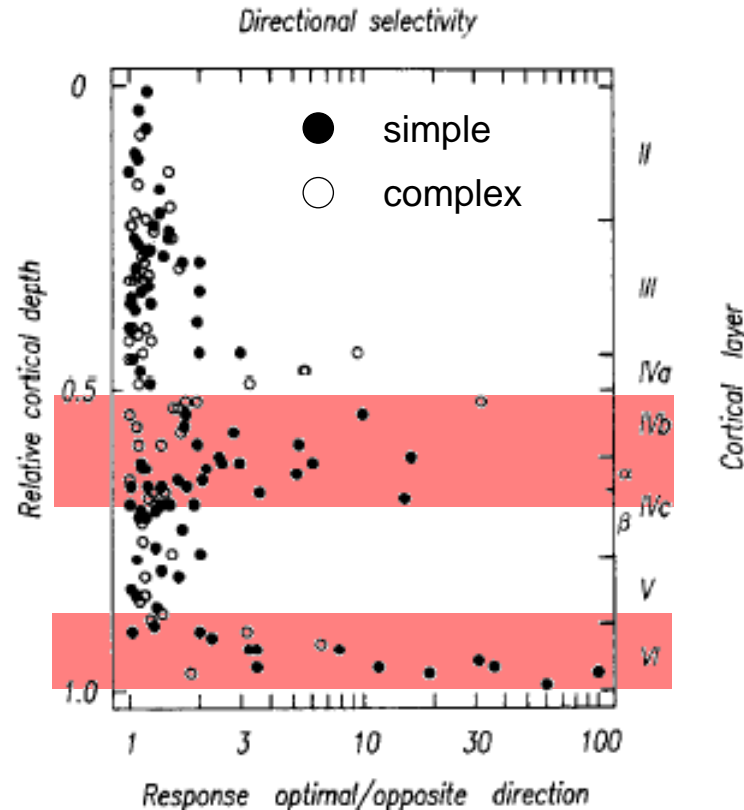


Dissection of the elements of the cascade model that create particular kinds of selectivity for the motion of plaids for five example cells ordered by pattern index (a–e). The first column shows the response of a version of the V1 stage of the model, without normalization, equivalent to the square root of the response of an energy model⁴.

(f) Plots illustrating the role of V1 normalization in the computation of pattern motion for the fifth example cell. Only in this final panel is direction-invariant pattern selectivity seen.

Rust, Mante, Simoncelli & Movshon (2006). How MT cells analyze the motion of visual patterns. *Nat. Neurosci.*, 9(11), 2006

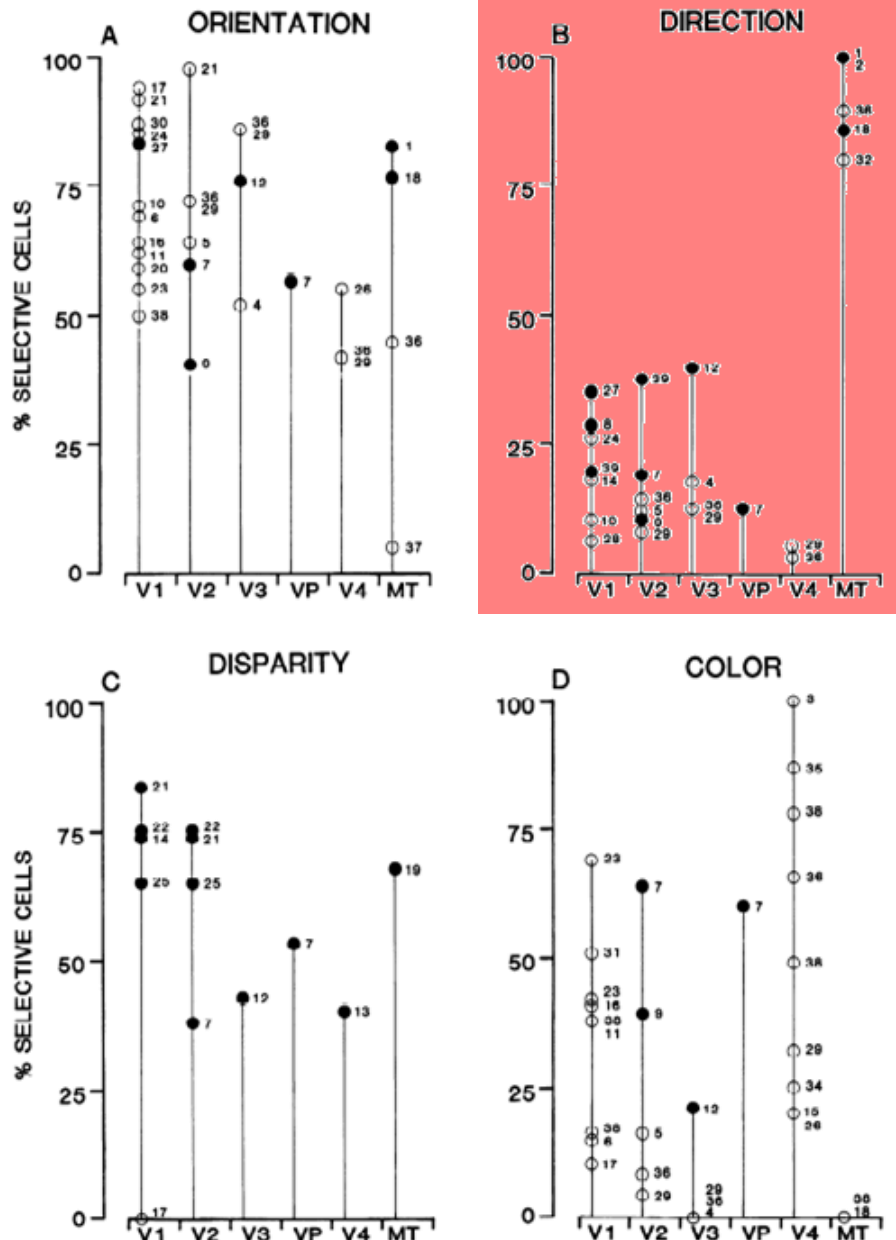
Directional preference of V1 macaque



Directional preference of 147 V1 macaque cells is plotted as a function of laminar position. Directional preference calculated as ratio of peak response in the preferred direction to the response in the non-preferred direction. Only cells in layer 6 and middle layer 4 show pronounced directional tuning. Twelve of the cells included in this distribution were non-oriented. Open symbols, 54 complex cells plus 3 nonlinear, non-oriented cells; closed symbols, 81 simple cells plus 9 linear non-oriented cells.

Hawken, Parker & Lund (1988). *J. Neurosci.*, 8(10), 3541-48.

Directional preference across visual areas of the macaque

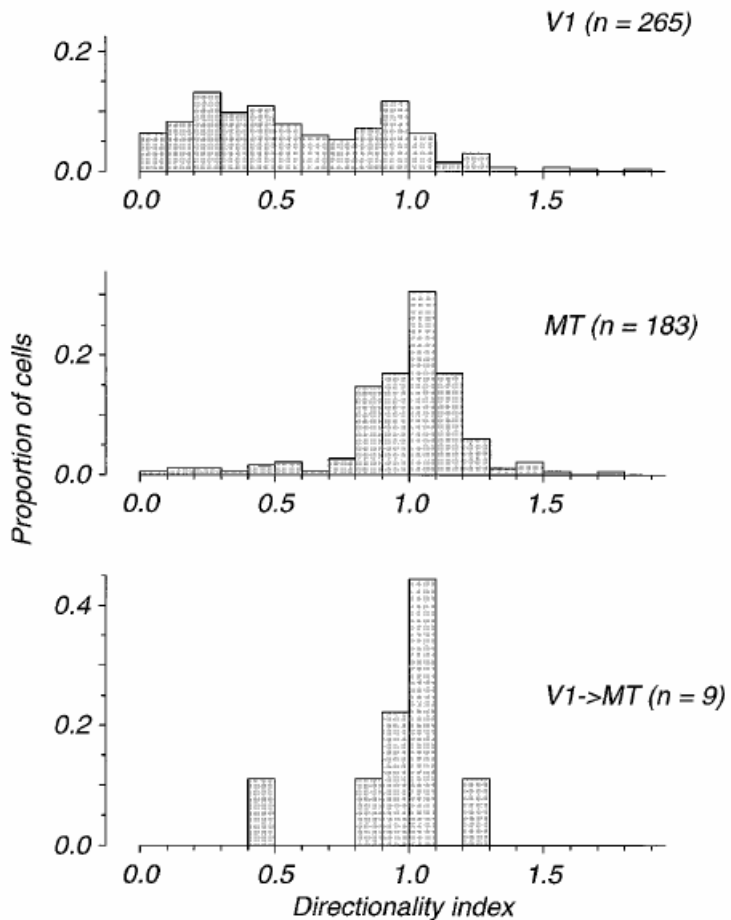


Comparison of neuronal selectivities across visual cortical areas. Estimates of the proportion of cells in different cortical areas selective for *A*, orientation; *B*, direction; *C*, binocular disparity; and *D*, color. Qualitative estimates indicated by open symbols and quantitative estimates by solid symbols. Numbers beside each symbol refer to individual published studies as indicated below.

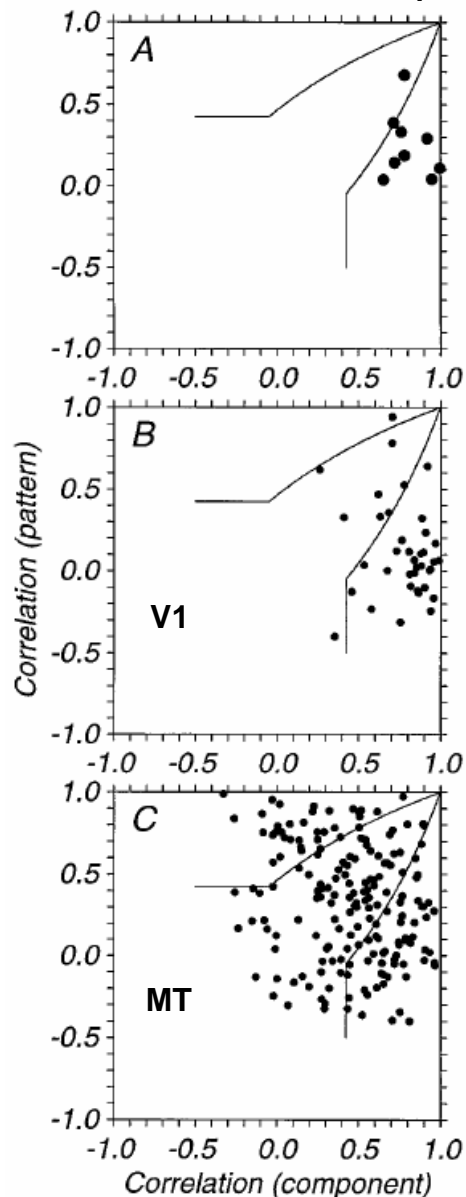
- | | |
|--|------------------------------|
| 1. Albright ('84) | 20. Poggio ('72) |
| 2. Albright et al. ('84) | 21. Poggio and Fischer ('77) |
| 3. Anderson et al. ('82) | 22. Poggio and Talbot ('81) |
| 4. Baizer ('82) | 23. Poggio et al. ('75) |
| 5. Baizer et al. ('77) | 24. Poggio et al. ('77) |
| 6. Bullier and Henry ('80) | 25. Poggio et al. ('85) |
| 7. Burkhalter and Van Essen ('86) | 26. Schein et al. ('82) |
| R. De Valois et al. ('82) | 27. Schiller et al. ('76) |
| 9. DeYoe and Van Essen ('85) | 28. Spinelli et al. ('70) |
| 10. Dow ('74) | 29. Van Essen and Zeki ('78) |
| 11. Dow and Gouras ('73) | 30. Wurtz ('69) |
| 12. Felleman and Van Essen (present study) | 31. Yates ('74) |
| 13. Felleman and Van Essen (unpublished) | 32. Zeki ('74) |
| 14. Fischer and Poggio ('79) | 33. Zeki ('73) |
| 15. Fischer et al. ('81) | 34. Zeki ('75) |
| 16. Gouras ('74) | 35. Zeki ('77) |
| 17. Hube1 and Wiesel ('68) | 36. Zeki ('78) |
| 18. Maunsell and Van Essen ('83a) | 37. Zeki ('80) |
| 19. Maunsell and Van Essen ('83b) | 38. Zeki ('83) |
| | 39. Foster et al. ('85) |

Felleman D.J & Van Essen D.C (1987). Receptive field properties in area V3A of Macaque monkey extrastriate cortex. *J. Neurophysiol.*, 57(4), 889-920.

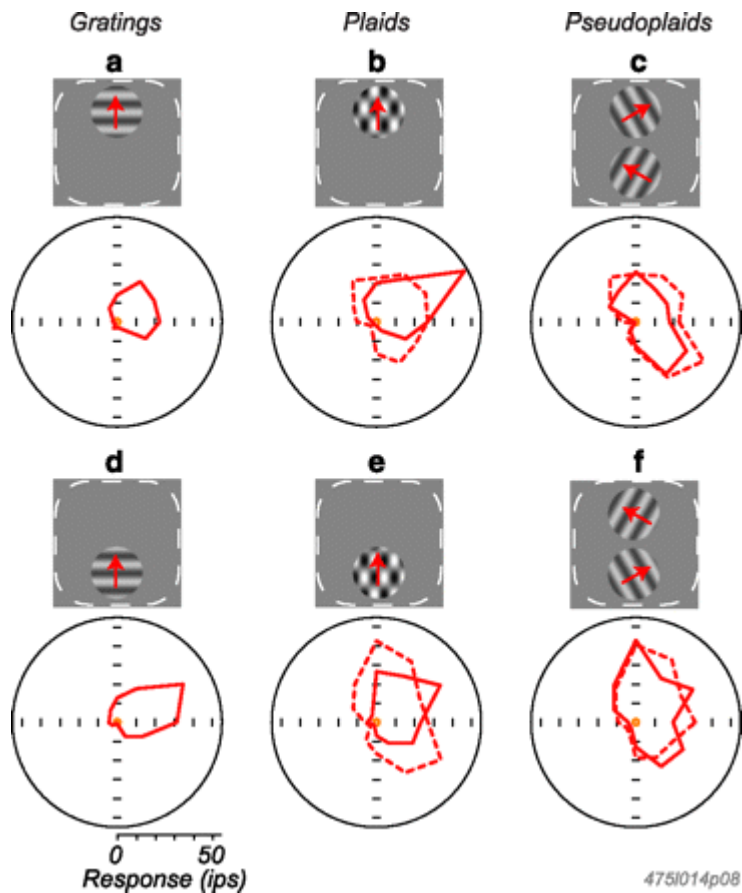
Directional preference in V1 & MT areas of the macaque



Frequency histograms of directionality indices for randomly sampled V1 neurons (*top*), randomly sampled MT neurons (*middle*), and V1 neurons antidromically activated from MT (*bottom*).

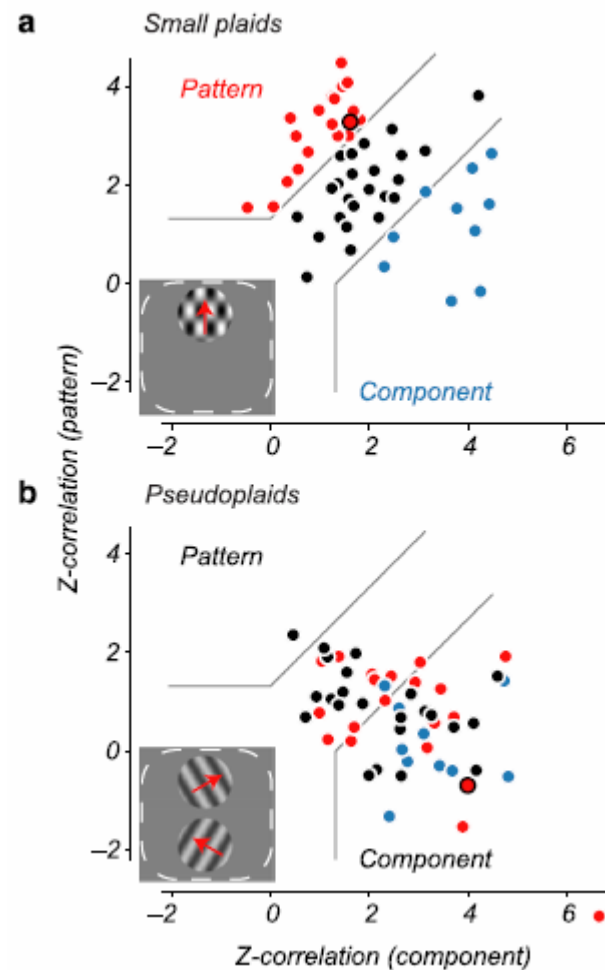


Scatterplot of the partial correlation coefficients calculated for each antidromically activated neuron. The abscissa shows the partial correlation between the data and the “component” prediction, whereas the ordinate shows the partial correlation between the data and the “pattern” prediction. The bullet-shaped contour divides this space into three regions of interest. Down and to the right is a region in which the correlation with the component prediction significantly exceeded the correlation with the pattern prediction or 0, whichever was larger. Neurons falling into this region most closely reflected the motion of the component gratings, and we consider such neurons to be component direction-selective. The converse relationship holds in the region up and to the left, and we consider neurons falling in this area to be pattern direction-selective. In between is a region in which cells cannot be classified as selective for either pattern or component motion. For cells in this region, neither correlation coefficient differed significantly from 0, or the two coefficients did not differ significantly from each other. For comparison, Figure 6, B and C, shows similar scatterplots for populations of neurons randomly sampled from V1 and MT, respectively. Overall, the distribution from the antidromically activated neurons appeared to be indistinguishable from that observed for V1 neurons (Fig. 6B) and was obviously different from the much broader distribution observed for MT neurons (Fig. 6C).



Responses of an MT cell to gratings, plaids, and pseudoplaids. Polar plots express cell response in spikes per second as distance from the origin, with the angle indicating the stimulus direction of motion. The small orange circles indicate spontaneous firing rate. **a, d**, Responses to a drifting grating covering one or the other of two patches within the receptive field, as indicated by the stimulus icons. **b, e**, Responses to the plaids created by summing two of the gratings tested in **a**, with orientations differing by 120° . Dashed red curves indicate the predicted response of a component-direction-selective cell. **c, f**, Responses to pseudoplaids obtained with gratings in the two patches arranged with a direction difference of $+120^\circ$ (**c**) or -120° (**f**).

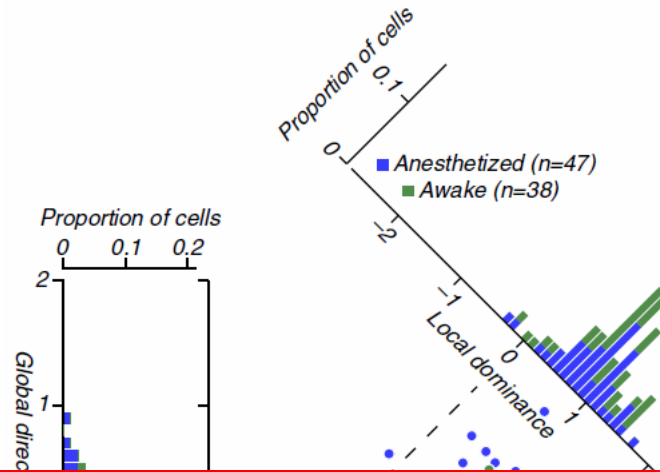
Majaj, N. J., Carandini, M. & Movshon, J. A. (2007). Motion integration in Macaque MT is local, not global. *J. Neuroscience*, 27, 366-370.



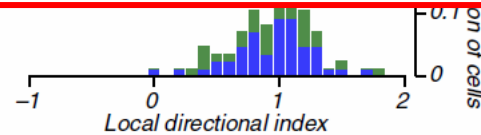
Summary of the results across the cell population. **a**, The degree to which cells are selective for the direction of a whole pattern or of the individual components as determined with small plaid stimuli. The Z-transformed partial correlations between the data and the “component” and “pattern” models are plotted against one another. Gray lines separate regions within which cells are classified as pattern-direction selective or component-direction selective, according to a conservative statistical criterion. Cells classified as pattern selective are indicated in red, as component selective in blue–green, and as unclassified by this method in black. **b**, A similar plot made from data taken from the same cells using pseudoplaids. The colors indicating the classification of the cells using small plaids are retained from **a**.



Hedges, Gartshteyn, Kohn, Rust, Shadlen, Newsome & Movshon (2011). Dissociation of Neuronal and Psychophysical Responses to Local and Global Motion, *Curr. Biol.*, 21(23), 2023-28.



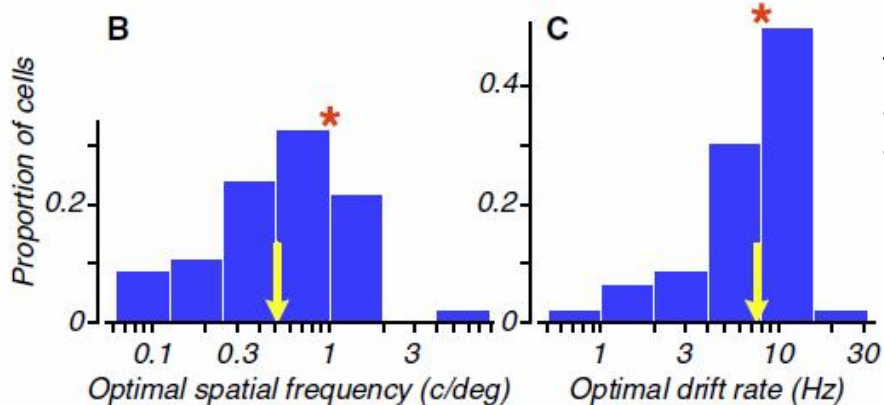
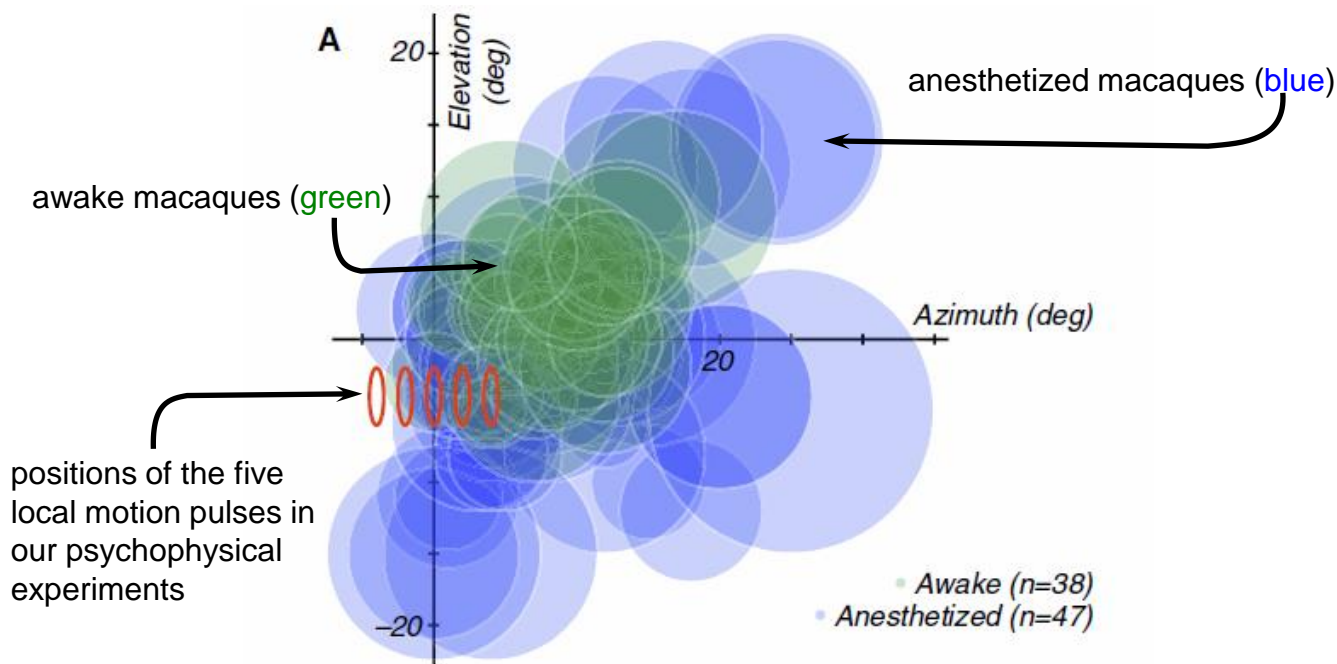
Although local motion perception might depend on MT signals, global motion perception depends on mechanisms qualitatively different from those in MT. Motion perception therefore does not depend on a single cortical area but reflects the action and interaction of multiple brain systems.



A Comparison of Directional Selectivity for Local and Global Components of Motion.

Local DI values are plotted against global DI values for 85 MT neurons. Data from anesthetized monkeys is in blue; data from awake monkeys is in green. The marginal distributions on the ordinate and abscissa capture the directional selectivity for the global and local motions, respectively. The oblique marginal distribution is of the difference between local and global DI, which we term local dominance.

Receptive Field Locations, Sizes, and Spatiotemporal Frequency Preferences for Neurons in MT



The distributions of optimal spatial frequency and drift rate for neurons recorded in anesthetized macaques. Yellow arrows indicate geometric means. The red asterisks indicate the values of each parameter used in psychophysical experiments.